AUTOPHAGY AND MUSCLE DYSFUNCTION IN LYSOSOMAL STORAGE DISEASES

AUTOPHAGY AND MYOGENIC DIFFERENTIATION IN LYSOSOMAL STORAGE DISEASES

By RON PADILLA (B.Sc.)

A Thesis Submitted to the School of Graduate Studies in
Partial Fulfillment of the
Requirements for the Degree Master of Science

McMaster University © Copyright by Ron F. Padilla, September 2018
All Rights Reserved

Master of Science (Biology, 2018)

McMaster University

Hamilton, Ontario, Canada

TITLE: Autophagy and Myogenic Differentiation in Lysosomal Storage Diseases

AUTHOR: Ron Padilla (B.Sc.) (McMaster University)

SUPERVISOR: Dr. Suleiman A. Igdoura (Ph.D.)

NUMBER OF PAGES: 90

Abstract

Lysosomal storage diseases (LSDs) are metabolic diseases which occur as a result of a deficiency of one of the essential lysosomal enzymes, called glycohydrolases. A mutation in the gene encoding one of these enzymes leads to an accumulation of unwanted substrates, resulting in a variety of clinical manifestations. A common symptom found in LSDs is skeletal muscle dysfunction, which includes muscle weakness, atrophy and loss of muscle mass. The genes for lysosomal hydrolases are well characterized; however, much less is known about how mutations in these genes affect the cell and lead to the muscle dysfunction observed. One pathway of interest is autophagy; it has been shown to be essential for maintenance of skeletal muscles. This study sought to investigate the impact of LSDs on autophagy and how this may potentiate muscle dysfunction. We utilized *in-vivo* and *in-vitro* models of Sialidosis, Sandhoff Disease, and GM_1-Gangliosidosis in order to assess autophagy and its impact on myogenic differentiation in skeletal muscles. Our results demonstrated that autophagy is induced upstream (ULK1 phosphorylation) but is inhibited at the autophagosome to lysosome fusion (p62 upregulation) in LSDs. We also found that myoblast fusion and myogenic differentiation are impaired. We conclude that blocking autophagy impairs myogenic differentiation, which potentiates the muscle dysfunction observed in LSDs. This work highlights autophagy as a new pathway of interest and possible therapeutic target to alleviate muscle dysfunction in LSDs, and other similar neurodegenerative diseases.

Acknowledgements

First and foremost, I would like to thank my supervisor Dr. Suleiman Igdoura. I have the utmost appreciation for his guidance and mentorship these past two years. He taught me how to conduct myself within the lab and has taught me how to succeed as a scientist. I will remember his teachings throughout my career. Next, I would like to thank past and current members of the Igdoura lab. I would like to thank Dr. Alex Hooper for his mentorship and continued technical advice during my two years. I would like to thank Kathryn Fisher, Solomiya Turchyn, Dana Yablonovich, and Emmanuel Sakaryan for all their help with my experiments and accompanying me within the lab. I will also remember our memories and laughs throughout these 2 years. I would like to thank Ish Jain, and other members of the Gupta and Schellhorn lab for the friendship and advice whenever I needed it.

Next, I would like to thank my girlfriend, Tamara. She has given me continued support and friendship for the past few years of my life, and I would have never applied to the McMaster graduate program without her. I would also like to thank my parents and my brothers for motivating and standing by me throughout my whole life. I am very lucky to have such endearing people in my life.

Table of Contents

List of Figures

Abbreviations

4EBP1	Eukaryotic translation initiation factor 4E (eIF4E)-binding protein 1
AD	Alzheimer's disease
AKT	Protein kinase B
AMBRA1	Autophagy and Beclin-1 Regulator 1
AMP	Adenosine monophosphate
AMPK	Adenosine monophosphate kinase
ATG	Autophagy-related protein
ATG7	Autophagy-related protein 7
ATG13	Autophagy-related protein 13
ATP	Adenosine-5'-triphosphate
B-gal	β-galactosidase
CAF	McMaster Central Animal Facility
CNS	Central nervous system
DMEM	Dulbecco's modified eagle medium
DNA	Deoxyribonucleic acid
EDTA	Ethylenediamine tetraacetic acid
eIF4E	Eukaryotic translation initiation factor 4E
FIP200	Kinase family interacting protein of 200 kD
GalNAc	N-acetylgalactosamine
GAPDH	Glyceraldehyde-3-phosphate dehydrogenase
GM1	Monosialotetrahexosylganglioside
GSLs	Glycosphingolipids
GTP	Guanosine-5'-triphosphate
HEPES	2-[4-(2-hydroxyethyl)piperazin-1-yl]ethanesulfonic acid
HEXA	β-hexosaminidase A
HEXB	β-hexosaminidase B
HRP	Horseradish peroxidise
IGF	Insulin-like growth hormone
LAMP1	Lysosome-associated membrane protein 1
LC3	Microtubule-associated protein 1A/1B-light chain 3
LSDs	Lysosomal storage diseases
LYNUS	Lysosome nutrient sensing machinery
MEK	Mitogen-activated protein kinase kinase
MHC	Myosin Heavy Chain
mTOR	Mechanistic target of rapamycin
mTORC1	mTOR Complex 1
mTORC2	mTOR Complex 2
Myf5	Myogenic factor 5
Neu1	Neuraminidase 1
p62/SQSTM1	Sequestosome 1
PCR	Polymerase chain reaction

PBS	Phosphate-buffered saline
PDK1	3-phosphoinositide-dependent kinase 1
PI3K	Phosphoinositide 3-kinase
PIP3	Phosphatidyl inositol 3,4,5 tri-phosphate
PPCA	Protective protein cathepsin A
RHEB	Ras homolog enriched in brain
RNA	Ribonucleic acid
RPS6	Ribosomal protein S6
siRNA	Small interfering RNA
TFEB	Transcription Factor EB
TSC2	Tuberous sclerosis complex 2
ULK1	Unc-51 Like Autophagy Activating Kinase 1
VPS34	Phosphatidylinositol 3-kinase

Declaration

All work was performed by Ron Padilla except the following:

1) Harvest and preparation of Sandhoff and wild-type mice cerebellum was performed by Dr. Alex Hooper.

Chapter 1: Introduction

1.1 Lysosomes

Lysosomes are highly acidic organelles found ubiquitously within eukaryotic cells (Mony et al., 2016). Lysosomes digest macromolecules and break them down to remove unwanted substrates, produce new basic building blocks, destroy pathogens and maintain the cell (Mony et al., 2016). Lysosomes have a single lipid bilayer membrane, which fuses with autophagosomes to degrade unwanted substrates (Mony et al., 2016). There are up to 60 different soluble acid glycohydrolases within the lysosome that are involved in the break-down different substrates (Mony et al., 2016). These hydrolases are active in low pH environments such as the lysosomal lumen (Mony et al., 2016). Biogenesis of lysosomes is regulated by several factors; however, one of the most essential of these regulators is the Transcription Factor EB (TFEB), (Settembre et al., 2012). In response to the availability of nutrients, TFEB controls autophagy through the positive regulation of lysosome biogenesis and autophagosome-lysosome fusion (Settembre et al., 2012). The Rag GTPase complex is responsible for sensing the availability of lysosomal amino acids as well as cellular stress (Settembre et al., 2012). In nutrient-rich conditions, the Rag GTPase complex activates mTORC1, which phosphorylates and inhibits TFEB (Settembre et al., 2012). Phosphorylation of TFEB prevents induction of lysosomal and autophagosome biogenesis, as well as autophagosome-lysosome fusion (Napolitano and Ballabio, 2016). During nutrient-poor conditions and lysosomal stress, mTORC1 is inhibited. Inhibition of mTORC1 results in the activation of TFEB and its translocation to the nucleus (Settembre

et al., 2012). In the nucleus, it positively regulates the formation of lysosomes and fusion with autophagosomes to complete autophagy (Settembre et al., 2012).

Autophagy is a catabolic process involved in the enzymatic break down of macromolecules through the fusion of autophagosomes with lysosomes (Dunlop and Tee, 2014). One subtype of autophagy is macroautophagy (Sandri, 2011). Macroautophagy, which will now be referred to as autophagy for the purpose of this study, is used to remove impaired organelles and unwanted proteins from the cell by breaking down these substrates to create new biomolecules (Carroll and Dunlop, 2017). The upstream regulation of lysosomes and autophagic influx is dependent on a number of stimuli (Dunlop and Tee, 2014). The availability of ATP, amino acids, fatty acids and nucleotides are important inputs in determining autophagic levels within the cell (Dunlop and Tee, 2013). Growth factor and hormonal inputs such as insulin and insulin-like growth factor (IGF) also play a significant role in regulating the catabolic activity of lysosomes (Dunlop and Tee, 2013).

Catabolic processes, such as autophagy, are regulated by the serine/threonine protein kinase mammalian target of rapamycin (mTOR) (Dunlop and Tee, 2014). mTOR is a signal integrator in which environmental inputs can converge and become integrated (Dunlop and Tee, 2014). These signals can come from the cytoplasm, plasma membrane, mitochondria, and the lysosome (Carroll and Dunlop, 2017). mTOR is found in two complexes; the first is mTOR complex 1 (mTORC1), which contains the rapamycin-associated protein of TOR (Raptor), and the second is mTOR complex 2 (mTORC2), which contains the rapamycin insensitive companion of TOR (Rictor) (Mendoza et al., 2011). mTORC1 is also a vital part of the anabolic process associated with promoting cell growth and proliferation

(Dunlop and Tee, 2014). Raptor enables the binding of mTORC1 to its multiple substrates, ultimately promoting cell growth and proliferation (Saxton and Sabatini, 2017). mTORC1 is inhibited by rapamycin; although mTORC2 is not affected, continued rapamycin treatment does slightly inhibit mTORC2, most likely due to its effects on mTORC1 (Saxton and Sabatini, 2017). Nutrients such as amino acids and glucose can induce the translocation of mTORC1 to the lysosomal surface where two protein complexes, the Ragulator/RAG-heterodimer, and the v-ATPase proton pump dock mTORC1 to form a multiprotein complex called lysosome nutrient sensing machinery or LYNUS (Mony et al., 2016). LYNUS is essential in the nutrient sensing of mTORC1 (Mony et al., 2016). Amino acids convert the Rag GTPases to their active state which promotes binding of mTORC1 to the lysosomal surface (Saxton and Sabatini, 2017). The lysosomal v-ATPase is responsible for sending signals to mTORC1 about the levels of amino acids in the lysosome lumen (Saxton and Sabatini, 2017). Amino acids generated by autophagy can sustain MTORC1 signalling; this is referred to as the "inside-out" model (Yu and Long, 2015). mTORC1 is inhibited during early stages of autophagy but is reactivated during later stages of due to new amino acids being created (Carroll and Dunlop, 2017). In the absence of amino acids, mTORC1 is inactivated and distributed throughout the cell (Newton et al., 2015). mTORC2 has an indirect role in the activation of mTORC1 via the Akt pathway (Dunlop and Tee, 2014). mTORC1 induces growth by phosphorylating ribosomal protein S6 (RPS6), and eukaryotic translation initiation factor 4E binding protin 1 (4EBP1) (Caroll and Dunlop, 2017). Phosphorylated RPS6KB1 activates RPS6 to enable initiation of mRNA translation.

Phosphorylation of 4EBP1 prevents its inhibition of EIF4E (eukaryotic translation initiation factor 4E), allowing initiation of translation (Newton et al., 2015).

When nutrients are abundant, mTORC1 inactivates autophagy to promote cell growth (Dunlop and Tee, 2014). In these conditions, growth factors activate phosphatidylinositol 3-kinase (PI3K), which generates phosphatidyl inositol 3,4,5 tri-phosphate (PIP3) to localize the protein kinase AKT to the plasma membrane where it is activated by 3-phosphoinositide-dependent kinase 1 (PDK1) and mTORC2 (Mendoza et al., 2011). Upon activation, AKT phosphorylates TSC2 (tuberous sclerosis complex 2), which prevents TSC2's inhibition of RHEB-GTP (Mendoza et al., 2011). RHEB-GTP is then recruited to the lysosome (Mendoza et al., 2011). Amino acids, which are detected by the amino acid sensing machinery in the lysosome, positively regulate mTORC1 through activation of Rag GTPases, which recruits mTORC1 to the lysosomal membrane where it is activated by co-localizing with RHEB-GTP (Mendoza et al., 2011). When mTORC1 is active, Raptor directly phosphorylates ULK1 and Atg13 within the ULK1/Atg13/FIP200 complex, thereby preventing ULK1 activation by adenosine monophosphate kinase (AMPK), and ultimately inhibiting autophagy (Ward et al., 2016). mTORC1 can also suppress the ULK1 complex by destabilizing it through the phosphorylation of autophagy/Beclin-1 regulator 1 (AMBRA1) (Dunlop and Tee, 2013). Phosphorylation of AMBRA1 by mTORC1 prevents ubiquitination of ULK1 on K63, which reduces ULK1 self-association and stability (Dunlop and Tee, 2014). Nevertheless, even when nutrients are plentiful, basal levels of autophagy is necessary in preventing the build-up of unwanted organelles (Dunlop and Tee, 2014).

Under nutrient-poor conditions, mTORC1 is inactivated and cannot phosphorylate ULK1 and Atg13 (Ward et al., 2016). A lack of amino acids detected within the lysosome prevent the activation of mTORC1 (Mendoza et al., 2011). AMPK is activated by sensing the low AMP: ATP levels within the cell, which can occur as a result of glucose deprivation and hypoxia (Mendoza et al., 2011, Ha et al., 2015). AMPK can inhibit mTORC1 through two pathways, by activating TSC2 or by directly phosphorylating mTORC1 (Saxton and Sabatini, 2017). AMPK can bind to mTORC1 and phosphorylate Raptor, thereby preventing ULK1 inactivation (Dunlop and Tee, 2014). Activation of TSC2 causes it to inhibit RHEB-GTP, which prevents mTORC1 activation at the lysosomal surface (Mendoza et al., 2011). Phosphorylation of ULK1 by AMPK initiates autophagy through the formation of autophagosomes (Laplante and Sabatini, 2012). Beclin-1 collaborates with the ULK1 complex to form the class III phosphatidylinositol 3-kinase (PI3K) which is necessary for nucleation and assembly of the phagophore membrane, resulting in the autophagosome (Wu et al., 2015). A complex consisting of VPS34, Beclin-1, Vps15, Ambra1 and Atg14 is activated by the ULK1/Atg13/FIP200 complex and induces the recruitment of microtubule-associated protein 1 light chain 3 (LC3-I) to the nascent autophagosome (Bonaldo and Sandri, 2013). LC3-I promotes phagopore elongation and its maturation to a complete sequestering vesicle in a process called lipidation (Bonaldo and Sandri, 2013). The autophagosome then loses its binding with the ATG proteins, while retaining LC3-I (Carroll and Dunlop, 2017). During formation and maturation of the autophagosome, LC3-I is converted to LC3-II by ATG proteins. LC3-II remains with the completed autophagosome (Menzies et al., 2015). Proteins and other cellular components

that are to be degraded are labelled with a polyubiquitin chain and delivered to the autophagosome by p62, a scaffolding protein (Bonaldo and Sandri, 2013). The autophagosome then fuses with the lysosome to form an autophagolysosome. As autophagy completes, p62 and the unwanted substrates are degraded (Bonaldo and Sandri, 2013). Through autophagy, the cell removes damaged mitochondria and misfolded proteins that can aggregate, regulate protein folding in the ER, and can impact DNA stability.

Impairment of autophagy can be detrimental to the cell. A lack of autophagy results in the accumulation of abnormal mitochondria which release proapoptotic factors and reactive oxygen species (Sandri, 2010). Furthermore, in the suppression of autophagy, polyubiquitins interact with p62 and oligomerize, resulting in an accumulation of ubiquitin-positive aggregates (Sandri, 2010). These aggregates are toxic to a number of organelles including mitochondria (Sandri, 2010).

1.2 Lysosomal Glycohydrolases

Glycosphingolipids (GSLs) are glycolipids found ubiquitously on the cell plasma membrane and is responsible for modulating signal pathways involved in cell proliferation, differentiation and survival (Magini et al., 2012). Gangliosides are part of a subgroup of GSLs which contain a ceramide backbone and a sialic acid residue (Schnaar et al., 2009). Regular turnover of gangliosides is essential to the cell and is carried out by the lysosome's glycohydrolases (Schnaar et al., 2009). Lysosomal glycohydrolases function in the degradation of gangliosides through cleavage of sugars and other residues (Schnaar et al.,

2009). Changes in ganglioside levels in the lysosome and plasma membrane have significant effects on cellular properties (Magini et al., 2012).

Neuraminidase-1 (Neu1), is a glycohydrolase found on the lysosomal membrane and is responsible for the removal of sialic acid residues from gangliosides and glycoproteins (Fanzani et al., 2012). Gangliosides function in several physiological processes such as adhesion and regulation of signal transduction within the nervous system and skeletal muscles (Fanzani et al., 2012). Newly formed Neu1 is transported to the lysosome where it is activated by the formation of a complex with β-galactosidase (β-gal) and protective protein/cathepsin A (PPCA) (Neves et al., 2015). This lysosomal hydrolase complex of Neu1, PPCA, and β-GAL is responsible for the coordinated degradation of oligosaccharides, glycoproteins, and other glycosylated molecules via cleavage of specific residues (Bonten et al., 2014). Neu1 is involved in a number of cellular processes including cell proliferation/differentiation, cell adhesion, catabolism of gangliosides, inflammation, cancer invasion and migration, formation of elastic fibers and immune response (D'Azzo et al., 2015). Neu1 regulates lysosomal exocytosis in cells by limiting the number of lysosomes which can fuse with the plasma membrane; it does so by removing the sialic acid residues found on lysosome-associated membrane protein 1 (LAMP1) (Neves et al., 2015). Without Neu1, increased levels of sialylated LAMP1 causes an increased turnover rate of the protein, allowing more lysosomes to dock at the plasma membrane (Bonten et al., 2014). Influx of Ca^{2+} then significantly enhances lysosomal exocytosis (Bonten et al., 2014). Abnormally high levels of lysosomal exocytosis lead to extra-cellular matrix remodelling, plasma membrane aberrant signalling, organ pathogenesis and changes in

cellular characteristics (D'Azzo et al., 2015). Neu1 has been observed to regulate skeletal muscle differentiation and regeneration. Several in vitro studies have reported a regulatory role of neu1 in myogenesis (Fanzani et al., 2012). In early stages of skeletal muscle myogenesis, neu1 is transiently upregulated (Fanzani et al., 2012). In later stages of myogenesis, a MEK-dependent mechanism downregulates neu1 expression (Champigny et al., 2005). Neu1 mRNA levels increased in the first 24h of differentiation, then decreased by 48h (Champigny et al., 2005). Champigny and associates (2005) observed that over-expression of neu1 levels inhibited myogenesis because neu1 altered myogenin and MHC activity. This suggests that modification to lysosomal enzyme expression has an impact on the expression of myogenic transcription factors.

β-galactosidase (β-gal) is a lysosomal enzyme responsible for hydrolyzing β-galactosyl residues from GM1-gangliosides and other glycoconjugates (Brunetti-Pierri and Scaglia, 2008). It functions in a complex with Neu1 at the lysosomal membrane (Bonten et al., 2014).

β-hexosaminidase, a glycohydrolase found on the lysosomal membrane, is responsible for the hydrolysis of GM2-gangliosides through the removal of terminal N-linked residues (Phaneuf et al., 1996). The *Hexb* gene encodes for the β-subunit of β-hexosaminidase, while *HexA* gene codes for the α-subunit (Sano et al., 1995). The α-subunit and β-subunit form three isoforms: αα, ββ, and αβ. Only the αβ and ββ isoforms are able to hydrolyze GM2-gangliosides (Pierson et al., 2013). The αβ heterodimer removes β-linked nonreducing terminal GalNAc from GM2 gangliosides (Chiricozzi et al., 2014).

1.3 Lysosomal Storage Diseases

In lysosomal storage diseases (LSDs), deficiency of important lysosomal glycohydrolases results in an accumulation of undigested macromolecules which leads to a variety of clinical manifestations (Lieberman et al., 2012). Mutations in genes coding for lysosomal hydrolases impairs the degradation of gangliosides resulting in their accumulation within the lysosome, which may affect the lysosomes function in other pathways. There are more than 50 lysosomal storage diseases, with the majority involving a defect in lysosomal hydrolases (Parkinson-Lawrence et al., 2010). However, dysfunction of other lysosomal proteins such as membrane, biogenesis, and transporter proteins can also result in LSD phenotypes (Parkinson-Lawrence et al., 2010). This suggests that any disruption in lysosomal protein function can be deleterious to the cell (Parkinson-Lawrence et al., 2010). At the cellular level, defects in lysosomal function can lead to an accumulation of undegraded substrates, abnormalities in cellular trafficking, disruption of the endocytic pathway and reduced clearance of autophagosome vacuoles which can be fatal to the cell (Parkinson-Lawrence et al., 2010). Lysosomal proteins are responsible for regulating large variety of substrates and the phenotype of the disease is classified according to the chemical properties of the substrate (Parenti et al., 2015). In LSDs, the deficient lysosomal glycohydrolase's function is not specific to a single substrate but rather specific sugar residue which may be found on several different substrates (Ballabio and Gieselmann, 2009). For example, a deficiency of β-gal in GM1-gangliosisodis results in the accumulation of sphingolipids, oligossacharides, and keratan sulphates (Ballabio and Gieselmann, 2009).

Lysosomes have a significant role in the autophagic pathway through their fusion with autophagosomes, suggesting that LSDs have an impact on autophagy (Lieberman et al., 2012). There has been recent interest in investigating autophagy in LSDs based on the theory that deficiencies of lysosomal storage enzymes may impact the lysosome's contribution to the autophagic process (Ballabio and Gieselmann, 2009). The rationale behind this was an accumulation of autophagic substrates was observed in the neurons of several LSDs, including GM1-gangliosidosis (Ballabio and Giselmann, 2009).

There are a number of clinical manifestations associated with LSDs and an overlap of phenotypes between each disease (Parenti et al., 2015). These phenotypes include visceral, ocular, skeletal, haematological, and neurological manifestations (Parenti et al., 2015). However, a common symptom observed within LSDs is skeletal muscle dysfunction. Adults with late onset versions of the disease have been observed to suffer from muscular weakness and atrophy (Parenti et al., 2015). LSD patients have been observed to have progressive loss of muscle strength and function (Prater et al., 2013). Muscle dysfunction has also been described in the three LSDs that are the focus of this study.

Three lysosomal storage diseases which vary in severity and age of onset are Sialidosis, Sandhoff disease, and GM1-gangliosidosis. Sialidosis, an autosomal recessive LSD, occurs as infantile or juvenile onset (D'Azzo et al., 2015). Sialidosis occurs because of genetic mutations at the Neu1 locus on chromosome 6p21 leading to a deficiency of Neu1 (Neves et al., 2015). The attenuated and non-neuropathic form is Type-I or cherry-red spot myoclonus syndrome (D'Azzo et al., 2015). This form of sialidosis displays some

residual activity of Neu1 (Franceschetti and Canafoglia, 2016). Clinical manifestations may remain undetectable early on in life; however, in the second decade of life, patients can suffer from gradual myoclonus, ataxia, gait abnormalities and macular degeneration (Bonten et al., 2014). Individuals with type-I sialidosis also experience gradual muscular dysfunction, myoclonus, ataxia and atrophy (Champigny et al., 2005). In severe cases, patients experience gradual and progressive muscle wasting rendering them confined to a wheelchair (Champigny et al., 2005). Interstitial vacoulated fibroblasts in skeletal muscle were found in a patient with type-II Sialidosis (Carpenter and Karpati, 1986). Muscle dysfunction has also been observed in mouse models of Sialidosis. During muscle regeneration in Neu1 deficient mice, myofiber maturation is slowed due to alterations in MyoD and myogenin expression (Neves et al., 2015). Skeletal muscle degeneration in Neu1 deficient mice occurs in association with abnormalities in extracellular matrix components and the accumulation of connective tissue in the muscle bed (Neves et al., 2015). Other symptoms indicating muscle atrophy in $Neu1^{-/-}$ mice includes expansion of epimysial and perimysial spaces, unusually high amounts of collagen deposits, invagination of the sarcolemma, infiltration of the muscle fibers by fibroblast-like cells and the cellular matrix (Zanoteli et al., 2010). The gastrocnemius muscle of $Neu1^{-/-}$ mice had significant amounts of connective tissue infiltrates (Zanoteli et al., 2010). These symptoms result in extensive muscle atrophy and consequently and leads to gradual motor impairment (Zanoteli et al., 2010). Hence, as Neu1-deficient mice grow older, the size of their muscle fibers and muscle to body weight ratio decreases significantly when compared to wild-type, indicating an impaired regeneration process (Zanoteli et al., 2010).

GM1-gangliosidosis presents as infantile, juvenile or adult onset (D'Azzo et al., 2015). GM1-gangliosidosis occurs due to the accumulation of GM1-gangliosides and related glycoconjugates in tissues and the CNS because of a deficiency of the β-galactosidase enzyme (D'Azzo et al., 2015). Mutations in the *GLB1* gene cause a deficiency of β-gal, thereby preventing the hydrolysis of GM1-gangliosides (D'Azzo et al., 2015). Clinical manifestations of the disease range from lag in motor and cognitive development to rapid deterioration of the nervous system depending on the clinical phenotype and age of onset (Brunetti-Pierri and Scaglia, 2008). Type-I or infantile onset patients have been observed to experience muscle weakness at the age of 6 months (Bonten et al., 2014). Case reports also indicate Type-II or juvenile-onset GM1-gangliosidosis patients experiencing mild to severe muscle atrophy and weakness (Yoshida et al., 1992, Brunneti-Pierri et al., 2008). β-gal$^{-/-}$ mice experience tremors, ataxia and abnormal gait coinciding with the progressive loss of motor function leading to paralysis of the hind limbs (Bonten et al., 2014). In the smooth muscle cells, electron microscope images showed vacuolization (Brunetti-Pierri and Scaglia, 2008). In mouse models of GM1-gangliosidosis, upregulation of autophagy has been observed (Takamura et al., 2008).

Sandhoff disease presents as infantile, juvenile or adult onset (D'Azzo et al., 2015). In Sandhoff disease, a mutation in the *Hexb* gene results in accumulation of GA2 and GM2 gangliosides in the central nervous system (Hooper et al., 2017). Sandhoff disease occurs because of a deficiency of the β-subunit of β-hexosaminidase which prevents the function of the αβ and ββ isozymes and results in accumulation of GM2 gangliosides in the lysosomes of neurons (Sango et al., 1996). Individuals with the disease are unable to

remove β-linked nonreducing GalNAc terminals because of a dysfunctional αβ and ββ isoform (Sango et al., 1996). Accumulation of glycolipids and other oligosaccharides result in the formation of multilayer structures which disrupt the function of neurons and visceral organs (Sango et al., 1996). Several clinical and ophthalmological manifestations, including motoneuronal and behavioural deficits, are observed in Sandhoff disease patients (Prada and Grabowski, 2013). Sandhoff disease patients have also shown symptoms of muscle dysfunction. A patient showing low hexosaminidase activity consistent with juvenile-onset GM2-gangliosidosis had progressive muscle weakness and atrophy (Pierson et al., 2013). *Hexb*$^{-/-}$ mice, a mouse model for Sandhoff disease, grow normally to adulthood. However, at 3 to 4 months post-birth, *Hexb*-/- mice begin to suffer from neurodegeneration, accompanied by motor dysfunction (Sango et al., 1996). Examination of mice cerebellum revealed storage of gangliosides which may indicate an impairment in autophagy (Sango et al., 1996).

Sialidosis, GM1-gangliosidosis, and Sandhoff disease is associated with a variety of symptoms including muscle weakness and atrophy. Enzyme replacement therapy for important lysosomal enzymes in LSDs has been found to restore lysosomal integrity in cardiac muscle, but not in skeletal muscle (Lieberman et al., 2012). Investigating the process of myogenesis, a process essential to muscle growth and regeneration, in LSDs may provide insight into the muscle dysfunction by LSD individuals.

1.4 Myogenesis in Skeletal Muscles

Myogenesis is the process of generating muscle tissue (Maltzahn et al., 2013). In adult skeletal muscles, quiescent satellite cells are maintained by Pax7, a paired-homeobox transcription factor necessary for satellite cell survival and function (Bentzinger et al., 2012). These satellite cells are located between the sarcolemma and basal lamina of the muscle fiber (Bharathy et al., 2013). Pax3, also a paired-homeobox transcription factor, controls the expression of muscle regulatory factors (MRFs), which are muscle specific basic helix-loop-helix transcription factors (Bentzinger et al., 2012). The MRFs which regulate myogenesis are Myf5, myoD, myogenin and MRF4. Upon muscle damage, Pax7 binds to the Myf5 promoter and induces the tri-methylation of histone H3 lysine 4 through the recruitment of the HMT complex Wdr5–Ash2L–MLL2 (Bharathy et al., 2013). When myogenesis begins, Myf5 is first transiently expressed at low levels and myoD expression is induced by Pax3 and Pax7 (Zanou and Gailly, 2013). Myf5 and myoD are required for determination of myogenic precursor cells (Bharathy et al., 2013). Myf5 first induces the proliferation of myoblasts, myoD then ceases myoblast proliferation and initiates migration and differentiation (Zanou and Gailly, 2013). Myogenin then activates myotube formation through the fusion of myoblasts and is involved in terminal differentiation (Zanou and Gailly, 2013). Myosin heavy chain is also involved in terminal differentiation (Champigny et al., 2005). Multinucleated myotubes then mature into myofibers (Sincennes et al., 2016).

Muscle tissue homeostasis is maintained by myogenesis (Bentzinger et al., 2012). The ability of muscles to regenerate, and avoid dysfunction or atrophy, is highly dependent on this process (Maltzahn et al., 2013). Findings have demonstrated that cellular

differentiation of skeletal muscle cells occurs following injury (Mu et al., 2011). Myogenic differentiation is important in maintaining healthy muscle cells, and muscle growth and regeneration (Chang et al., 2016). In healthy muscles, satellite cells proliferate into myoblasts and then fuse together into myotubes in order to regenerate muscle tissue (Chang et al., 2016). Muscle growth in the early stages after birth is dependent on fusion of satellite muscle cells to form an increasing number of multinucleated muscle cells (Schiaffino et al., 2013). Hence, an inadequate expression of MRFs, such as myogenin, prevents the proper formation of myofibers (Bharathy et al., 2013).

1.5 Autophagy in LSDs

Autophagy has been observed to play a significant role in the differentiation of a number of cell types. During the early stages of white adipocyte differentiation, autophagy and mRNA expression of autophagic genes are upregulated (Skop et al., 2014). Evidence suggests that autophagy also facilitates myofibroblast differentiation (Bernard et al., 2014). More significantly, autophagy is a key regulator of skeletal muscle differentiation and basal levels are necessary for proper removal of unwanted proteins (Bonaldo and Sandri, 2013). Autophagy is essential for muscle cell differentiation and may be necessary during myoblast fusion for the elimination of pre-existing structures such as organelles (Fortini et al., 2016). Autophagy is crucial for myoblast remodelling during differentiation and has been shown to degrade cell cytoplasm and organelles (Fanzani et al., 2012). It has been observed to be induced during myogenesis. Since p62 is observed to significantly decrease as myogenic differentiation of C2C12 progresses, it suggests that autophagy is occurring

during myogenesis (McMillan and Quadrilatero, 2014). Further evidence for the induction of autophagy is the significantly increased ratio of LC3-II over LC3-I (McMillan and Quadrilatero, 2014). Studies have also found that inhibition of autophagy has a negative impact on myogenic differentiation. 3MA-inhibition of autophagy impaired myoblast differentiation and fusion by delaying myogenin and MHC expression (McMillan and Quadrilatero, 2014). The fusion index significantly decreased in Beclin-1-knockdown C2C12 cells at the 48-hour and 72-hour mark of differentiation (McMillan and Quadrilatero, 2014). Thus, these studies indicate that autophagy is required to maintain muscle integrity because the ubiquitin-proteasome and autophagy-lysosome are the major pathways which regulate the degradation of muscle proteins (Masiero et al., 2009, Sandri, 2013).

A common characteristic observed in lysosomal storage diseases and neurodegenerative diseases, such as Parkinson's disease, is an impairment in the process of autophagy (Poewe et al., 2017). Autophagic substrates have been observed in the brains of LSD individuals (Menzies et al., 2015). *In-vitro* experiments of LSDs showed an accumulation of autophagosomes and lysosomes (Menzies et al., 2015). Increased expression of p62 was observed in the fibroblasts of several lysosomal storage diseases (Vergarajauregui and Puertollano, 2008). An accumulation of p62 indicates a block in autophagy because during autophagic turnover, p62 is degraded along with the unwanted substrates.

1.6 Autophagy Impairment and Muscle Dysfunction

When the rate of protein degradation is higher than the rate of protein synthesis, muscle atrophy occurs (Sandri, 2013). A net loss of proteins, organelles and cytoplasm leads to a decrease in myofiber size resulting in muscle atrophy (Sandri, 2013). The autophagy-lysosome system has been observed to play a role in muscle atrophy (Sandri, 2010). Although excess autophagy results in muscle loss, complete inhibition of autophagy also leads to muscle atrophy (Sandri, 2010). Deletion of an autophagy enzyme, Atg7, prevented vesicle formation in skeletal muscles and resulted in muscle weakness, atrophy and myopathy (Sandri, 2010). A lack of autophagy results in the accumulation of abnormal mitochondria which release proapoptotic factors and reactive oxygen species (Sandri, 2010). A build-up of abnormal mitochondria can also result in impaired mitochondrial function (Ballabio and Gieselmann, 2009). Furthermore, in the suppression of autophagy, polyubiquitins interact with p62 and oligomerize, resulting in an accumulation of ubiquitin-positive aggregates (Sandri, 2010). These aggregates are toxic to a number of organelles including mitochondria (Sandri, 2010). Atg7 KO mice had an accumulation of abnormal mitochondria, sarcoplasmic reticulum distension, and disorganization of sarcomeres within their skeletal muscles (Fanzani et al., 2015). Autophagy plays a dual role in the maintenance of skeletal muscles; basal levels are necessary for proper removal of unwanted proteins and cell components, but overexpression can lead to an excess in the removal of necessary cellular components leading to muscle wasting (Bonaldo and Sandri, 2013).

Studies have observed muscle weakness and atrophy as a common symptom in both lysosomal storage diseases, such as Sialidosis and Sandhoff disease, and neurodegenerative

diseases such as Parkinson's disease (Jeyakumar et al., 1999, D'azzo et al., 2015, Peker et al., 2018). Previous studies have also demonstrated skeletal muscle dysfunction in LSD mouse models as a result of impaired autophagy. In Danon's disease, Lamp-2 deficient mice showed extensive accumulation of autophagic vacuoles in skeletal muscles (Tanaka et al., 2000). In an LSD mouse model of Pompe disease, autophagic accumulation was observed in the skeletal muscles of 5-month-old mice (Lieberman et al., 2012). An excess of autophagy proteins was observed, indicating an upregulation of autophagy; however, the skeletal muscle phenotype displayed was deemed to be caused by the impairment of autophagic flux as indicated by the accumulation of the autophagic substrate, p62 (Lieberman et al., 2012). This block of autophagic turnover is suggested to be one of the primary causes of the loss of skeletal muscle fibers, resulting in muscle dysfunction (Lieberman et al., 2012). However, how this block of autophagic turnover results in skeletal muscle loss is largely unknown.

1.7 Rationale and Objectives

LSDs have been identified and their mutations characterized (Ballabio and Giselmann, 2009). The clinical manifestations associated with each LSD have also been identified. However, we still lack knowledge of the relevant events leading from the disease-causing mutations to the symptoms of the disease. Previous studies have presented muscle dysfunction as a common manifestation in several LSDs including Sialidosis, Sandhoff's disease and GM1-gangliosidosis. However, the cause of the muscle dysfunction observed in LSDs is largely unknown. Studies have also depicted an impairment in

autophagy within LSD individuals, but has yet to be investigated as a possible cause and therapeutic target for the muscle dysfunction observed in individuals with LSDs. We thus aimed to understand the link between autophagy and myogenic differentiation using *in-vivo* and *in-vitro* models of LSDs. Since myogenesis, or myogenic differentiation, is such an essential process in muscle growth and regeneration, we decided to investigate the effect of LSDs on this pathway. This will allow us to determine a possible mechanism by which impaired autophagy leads to muscle dysfunction. We hypothesized that impaired autophagy in the lysosomal storage diseases, Sialidosis, Sandhoff's disease, and GM1-gangliosidosis, disrupts myogenic differentiation, which ultimately potentiates muscle dysfunction.

Objectives

1) Previously outlined studies have observed an impairment in autophagy in LSDs. Preliminary experiments have also indicated that autophagy is also impaired in LSD cells (Igdoura, unpublished). To verify these studies, we determined the state of autophagy in an LSD mouse model for Sandhoff Disease. Sandhoff ($Hexb^{-/-}$) mice have been previously recognized as a suitable model for Sandhoff disease (Hooper et al., 2017). Since clinical manifestations of LSDs begin in the brain then cascades into the rest of the body as neuroinflammatory effects, we looked at the induction of autophagy within Sandhoff mice cerebellum and compared it with control mice ($Hexb^{+/+}$). The induction of autophagy through the mTOR pathway, phagosome/lysosome fusion and the class III PI3 kinase pathway in the cerebellum was assessed using Western Blots. The expression levels of phospho-mTOR/mTOR

(Ser2448), phospho-ULK1/ULK1 (Ser757), Beclin-1, and p62 were measured. We analyzed the cerebellum first in order to develop a baseline for the state of autophagy in our LSD mouse model.

2) To examine the state of autophagy and myogenic differentiation in LSD muscle tissue, we analyzed the soleus muscle of Sandhoff and B10.SM mice (Sialidosis mouse model). Muscle regeneration and myogenesis studies have been previously conducted on the soleus muscle (Yusuf and Brand-Saberi, 2012). The induction of autophagy was assessed using western blot analysis of autophagy markers. Markers of terminal myogenic differentiation were also analyzed through western blot. This study will allow us to determine the effect of autophagy on the muscle tissue in an LSD *in-vivo* model.

3) An *in vitro* system using C2C12 mouse myoblasts was used in order to observe the impact of a deficiency of important lysosomal enzymes on autophagy and myogenic differentiation. Since lysosomal enzymes are essential to the lysosome, it is likely they have an impact on autophagy as well. Abnormal levels of lysosomal enzymes, whether overexpression or deficiency, may impair autophagy, which has negative consequences on myogenic differentiation. For example, overexpression of Neu1resulted in the down-regulation of myogenin and in the inhibition of C2C12 differentiation (Champigny et al., 2005). The C2C12 cell line is a good model of mouse myoblasts since it expresses characteristic muscle markers upon

differentiation and has several advantages over primary myoblasts, namely greater accessibility and homogeneity. Furthermore, myoblasts can proliferate and induced into myotubes over many passages (Sincennes et al., 2016). In order to examine the impact of lysosomal enzymes on autophagy and on muscle regulatory factors mediating fusion and myotube formation, neuraminidase-1, β-hexosaminidase subunit β (*Hexb*), and β-galactosidase expression was knocked down in C2C12 myoblasts through siRNA transfections. Transfected cells were incubated in differentiating media (DMEM with 2% horse serum, 1% penicillin/streptomycin) and allowed to differentiate for 120hours. The cells were then analyzed for autophagy and myogenic differentiation markers using Western blots, stereological counting, and immunocytochemistry.

Chapter 2: Methods

2.1 Mice

Experiments on mice were performed according to an animal utilization protocol (AUP) in line with the Ontario for Research Act requirements and the Canadian Council on Animal Care (CCAC). *Hexb*$^{-/-}$ mice on a C57BL/6 background were generously donated by Dr. R. Gravel (University of Calgary, Calgary, AB, Canada). *Hexb*$^{-/-}$ mice have been acknowledged as a suitable mouse model for Sandhoff Disease and have been previously characterized (Phaneuf et al., 1996). *Hexb*$^{-/-}$ mice were bred in the McMaster Central Animal Facility (CAF) and were weaned at 21 days of age. These mice display no symptoms until the normal *Hexb*$^{-/-}$ endpoint of 120-130 days. *Neu1*^{hypo} (B10.SM) mice, which are sialidase mutants backcrossed 10 times against a C57BL/6 background, were used for similar experiments as the *Hexb*$^{-/-}$ mice. B10.SM and the C56BL/6 wild-type mice were kept and bred in the CAF.

2.2 Genotyping

Hexb$^{-/-}$ mice were placed under gaseous anesthesia using Isoflurane (Fresenius Kabi, B121G16B) and tagged with ear tags and tailed in the CAF for genotyping. Marcaine was applied on the tail prior to tailing, and VetBond (1469SB) was applied afterwards. Tail samples were brought to the lab for lysis in Tail Lysis Buffer (Viagen, 102-T) and Proteinase K, and incubated at 55^{o}C overnight. The following day, the tails were further incubated at 85^{o}C for 45 minutes. The DNA from the tail samples are diluted and prepared

for PCR. *Hexb* genotypes were determined with the following PCR primers: WT-Forward, GGTTTCTACAAGAGACATCATGGC; KO-Forward, GATATTGCTGAAGAGCTTG-GCGGC; Reverse, CAATCGGTGCTTACAGGTTTCATC. The PCR program in the Thermocycler (Eppendorf, Mastercycler) denatured DNA at 94° for 4 min, then cycled 94°, 60°, 72°, 30 seconds each for 40 cycles. A final extension was done at 72° for 7 minutes. Following PCR, the samples were run under gel-electrophoresis at 100V for 75 minutes and the *Hexb* genotype of each mice was determined.

2.3 Tissue Harvest

Hexb$^{-/-}$ and B10.SM mice at approximately 120 days of age were dissected and perfused with 1X Dulbecco's phosphate-buffered saline (DPBS) (Gibco, 14190250) via intracardiac injection. The cerebellum and the soleus muscle tissue were harvested into 1.5mL microcentrifuge tubes and placed into liquid nitrogen. The cerebellum and soleus muscle were lysed in RIPA (50 mM Tris, 165 mM NaCl, 1% Nonidet P-40, 0.01% sodium dodecyl sulfate, 0.5% Sodium deoxycolate, pH 8.0) buffer with EDTA and phosphate inhibitors (Complete Mini, Roche, 04693124001). The tissue lysates were sonicated using the Sonicator XL 2020 (Heat Systems Inc., Duty 20%, Output 4).

2.4 Cell Culture

C2C12 mouse myoblast cells were incubated in a 37 ^{o}C humidified incubator with 21% O_2 and 5% CO_2. Proliferating C2C12 cells were cultured in Dulbecco's modified eagle medium (DMEM) (Gibco, 11965084) supplemented with 10% Fetal Bovine Serum (FBS)

(Gibco, 12483020), 1% penicillin/streptomycin (P/S) (Invitrogen, 15140122), and 0.1% fungizone (Invitrogen, #15290018).

2.5 siRNA Transfections

One day prior to transfections, C2C12 cells were plated in 6-well and 24-well cell culture-treated plates. At the day of transfection, C2C12 myoblasts were approximately 70-80% confluent. The DMEM culture media in the plates was replaced with OPTI-MEM (Gibco, 31985088). The *Silencer Select* siRNAs were incubated with Lipofectamine 3000 Reagent (Invitrogen, L3000001), the reagent used to deliver the siRNAs within the cell, at room temperature for 15 minutes. Cells were transfected, in a drop-wise manner, with siRNA to knockdown *Neu1* (Ambion, s70482), *Hexb* (s67479), *Glb1* (s62967), and a negative-control siRNA (Ambion, 4611). 30µg of siRNA and 6 µL of Lipofectamine 3000 were added to each plate in the 6-well plates. 5µg of siRNA and 1µL of Lipofectamine 3000 were added to the 24-well plates. The plates were incubated in the transfection media for 24 hours. After 24 hours, the transfection OPTI-MEM media was replaced with complete DMEM. Transfected cells were then allowed to proliferate for 24 hours or until they reached approximately 90% confluency.

2.6 Differentiation

Once the cells had reached 90% confluency post-transfection, they were differentiated in DMEM supplemented with 2% Horse Serum (Gibco, 16050130) and 1% penicillin/streptomycin. Cells were differentiated for 120 hours, with the differentiation

media being refreshed every 24 hours. After 120h, the 6-well plates were rinsed with cold DPBS and lysed in RIPA buffer containing protease inhibitors and EDTA.

2.7 Differentiation Index

In order to assess cell fusion and myotube formation, 5 random areas for each well in the 6-well plates were imaged under an inverted microscope (Zeiss, Axiovert 25) and the number of cells and nuclei within each cell was counted. Each treatment had four wells for a total of 20 imaged areas per treatment. The cells were observed at 120h post-differentiation and imaged under 400x magnification. The percentage of multinucleated cells over the total number of cells in each image was calculated.

2.8 Protein Assay

The total protein concentration of the soleus muscle and C2C12 cell lysates were determined using the DC Protein Assay (Bio-Rad, 5000111). Duplicates of each sample and Bovine Serum Albumin (BSA) (NEB, 9998) standards were placed in a 96-well microplate. The DC Protein Assay reagents were added, and the plate was incubated for 15 minutes at room temperature. Total protein concentration was determined using a microplate reader (SpectraMax Plus 384).

2.9 Western Blot

Western blots were performed on cerebellum (prepared by Dr. Alex Hooper, McMaster University) and soleus muscle lysates from *Hexb*$^{+/+}$ and *Hexb*$^{-/-}$ mice. Western

blots were also used for protein analysis of B10.SM soleus muscle and C2C12 cell lysates. 6x Laemmli Sample Buffer (0.5M Tris pH 6.8, SDS, Glycerol, DTT (600mM), 0.3% Bromophenol Blue) was added to each sample. The samples were then heated at 100^{o}C for 5 minutes. A mini SDS-PAGE apparatus was filled with Running Buffer (Glycine, Tris, SDS). The gels used were 4-15% Mini-PROTEAN TGX Precast Protein Gels (Bio-Rad, 4561083). 20µg of protein for each sample was loaded into the gel and ran for 90 minutes at 90V room temperature. In a transfer apparatus containing cold transfer buffer (Glycine, Tris, SDS), the gel was transferred onto a nitrocellulose membrane for 1h at 100V and 4 ^{o}C. After the transfer, the membrane was blocked with 5% cow milk (Carnation) in Tris-buffered saline containing 0.5% Tween-20 (TBST). The membrane was incubated in a primary antibody aliquot suspended in 5% milk TBST (1:500) overnight at 4 ^{o}C. The primary antibody was retrieved and re-stored in the -20 ^{o}C freezer, and the membrane was washed 4 times with TBST for 10 minutes. The membrane was incubated in IgG-HRP conjugated secondary antibody suspended in 5% milk TSBT (1:2000) for 1 hour at room temperature. The secondary antibody was removed, and the membrane was washed with TBST 6 times for 10 minutes. The washes were removed, and the membrane was incubated in Amersham ECL Western Blotting Detection Reagents (GE Healthcare, RPN2106) for 2 minutes. The membrane was exposed on an Amersham Hyperfilm ECL film (GE Healthcare, 28906839) for varying exposure times and placed into a film developer. After the films were developed, the membrane was rinsed in ddH_2O, washed with TBST for 5 minutes, stripped with stripping buffer (Glycine, SDS, Tween-20, pH 2.2) 2 times 10

minutes each, and washed with TBST for 5 minutes. The membrane was then incubated with another primary antibody overnight or stored in 4 ^{o}C.

2.10 Quantification of Western Blots

Films of the western blots were scanned and saved as JPEG files. Densitometry was measured using the gel analysis feature on ImageJ (v1.46r, NIH, USA). The free hand tool was used to outline a thin area on the bands and the mean and integrated density was determined by ImageJ. The integrated density value of each band was divided by the corresponding density value for GAPDH in order to represent normalized relative protein expression in each sample.

2.11 Immunocytochemistry

Prior to cell plating and siRNA transfections, coverslips were added to each well of a 24-well plate. C2C12 cells were cultured onto the 12mm circle coverslips (Fisher Scientific, 12-545-80) and transfected with siRNAs. After siRNA transfections and 120 hours of differentiation, C2C12 cells in the 24-well plates were fixed in formaldehyde. The differentiation media was removed from the wells and the cells were washed with cold DPBS 2 times for 5 minutes each. The cells were fixed in 3.5% formaldehyde in DPBS for 1 hour at room temperature. The formaldehyde was removed, and the cells were permeabilized with 0.5% Triton-X 100 (Bio-Rad, 161-0407) in DPBS for 1 hour. The cells were blocked with 10% Goat Serum in DBPS for 1 hour. The 10% Goat Serum was removed and 100µL of a solution containing two different primary antibodies, from

different source animals, suspended in 10% Goat Serum in DPBS at a concentration of 1:200 was added to each well. The plate was covered in parafilm and incubated at 4 ^{o}C overnight. The following day, the primary antibodies were removed, and the cells washed with DPBS + 0.05% Tween-20 (DPBS-T) 6 times 5 minutes each at room temperature. The corresponding mixture of secondary fluorescent antibodies were suspended in DPBS with 10% Goat Serum at a concentration of 1:400 and centrifuged at 16,400 rpm for 10 min. to remove any unbound fluorophore. 100µL of the mixture of secondary fluorescent antibodies was added to each respective well and incubated for 1 hour at room temperature. The secondary antibodies were removed, and the wells were washed with DBPS-T for 6 more times for 5 minutes. The cells were stained with 100µL of DAPI (Invitrogen, D1306) for staining of nuclei and incubated in darkness for 5 minutes. The wells were washed with DBPS-T 2 times for 5 minutes and 1 mL DPBS was left in the wells for mounting. The cover glasses were removed, rinsed in double distilled H_2O and mounted with ProLong Gold Antifade Reagent (Life Technologies, P36930) on a microscope slide. The slides were allowed to dry for 1 hour at room temperature and stored in -20 ^{o}C.

2.12 Fluorescence Microscopy

Immunocytochemistry slides were viewed under a fluorescent microscope (Zeiss, Axiovert200) under the 40x lens. Fluorescence images presenting the localisation of nuclei, autophagy, and muscle differentiation markers were taken and compared for each treatment. Images and fluorescent overlays were generated using the Leica AxioVision software (V4.8.2.0).

2.13 Chemicals and Antibodies

C2C12 cells were cultured using DMEM supplemented with 10% FBS, 1% P/S, and 0.1% fungizone. Cells were passaged with 1X DPBS and 0.25% Trypsin-EDTA (Gibco, 15400054). siRNA transfections were completed in OPTI-MEM media.

For western blots, the primary antibodies used were: mouse monoclonal Neu1 (Santa Cruz, sc-166824), polyclonal rabbit p62 (Cell Signalling, 5114S), polyclonal rabbit LC3A/B (Cell Signalling, 4108), polyclonal rabbit p-ULK1 (Ser757) (Cell Signalling, 6888), monocloal rabbit p-ULK1 (Ser555) (Cell Signalling, 5869), monoclonal rabbit ULK1 (Cell Signalling , 8054), monoclonal rabbit Beclin-1 (Cell Signalling, 3495), polyclonal rabbit TFEB (Cell Signalling, 4240), Lamp2, Lamp2a, monoclonal rabbit mTOR (Cell Signalling, 2983), monoclonal rabbit p-mTOR (Ser2448) (Cell Signalling, 5536), monoclonal mouse Myogenin (Hybridoma Bank, F5D-C), mouse monoclonal MHC (Hybridoma Bank, 10F5-S), and GAPDH (R&D Systems, #AF5718). The respective secondary antibodies were: anti-rabbit IgG HRP-linked (Cell Signalling, 7074S), anti-mouse IgG HRP-linked (Cell Signalling, 7076S), and donkey anti-goat IgG-HRP (Santa Cruz, sc-2020). For immunocytochemistry experiments, the primary antibodies used were: polyclonal rabbit LC3A/B (Cell Signalling, 4108), monoclonal mouse Myogenin (Hybridoma Bank, F5D-C) and mouse monoclonal MHC (Hybridoma Bank, 10F5-S. The respective secondary antibodies were: Alexa Fluor 488 goat anti-rabbit IgG (Invitrogen, A11008) and Alex Fluor 647 anti-mouse IgG (Invitrogen, A10475). Cells were also stained with DAPI.

2.14 Statistical Analysis

t-tests were used to determine significant difference between means at $P<0.05$ for data sets with two groups. One-way ANOVA was used to determine significant difference between means at $P<0.05$ for data sets with three groups. All statistical analyses were performed using GraphPad Prism 6 (V6.01).

Chapter 3: Results

3.1 Autophagy is induced in Sandhoff mice cerebellum.

Previous studies have observed an induction and impairment of autophagy in LSDs (Poewe et al., 2017). Preliminary experiments in the Igdoura Lab have revealed that LSD cells have shown a defect in autophagy. In order to assess the state of autophagy and the role of mTOR in lysosomal storage disorders using an *in-vivo* model, the expression levels of autophagy markers were observed in the cerebellum of Sandhoff mice ($Hexb^{-/-}$) and compared to wild-type ($Hexb^{+/+}$) mice (Fig. 1). We hypothesized that autophagy would be induced in the brain due to the cellular stress experienced by brain cells of individuals with LSDs (Prada and Grabowski, 2013). We examined the cerebellum of Sandhoff mice to develop a baseline for the effect of LSDs on autophagy because clinical manifestations of LSDs begin in the cerebellum and cascades into the rest of the body as neuroinflammatory effects (Prada and Grabowski, 2013).

Expression levels of phospho-ULK1, ULK1, Beclin-1, mTOR, and TFEB in Sandhoff ($Hexb^{-/-}$) and wild-type ($Hexb^{+/+}$) cerebellum lysates were examined using western blot to investigate levels of autophagy induction (Fig. 1A). ULK1 is a key component in the initiation of autophagy; when ULK1 is phosphorylated by mTORC1 at Serine 757, ULK1 is inhibited and autophagy is downregulated. However, under conditions of low nutrients and cellular stress, AMPK phosphorylates ULK1 at Serine 555 to induce autophagy. Phospho-ULK1 (Ser757) and total-ULK1 expression relative to GAPDH was significantly decreased in Sandhoff mice cerebellum compared to wild-type, which may

indicate a reduced level of total ULK1, including phosphorylated ULK1, within Sandhoff mice cerebellum (Fig. 1B). Western blot analysis also showed that expression of phosphorylated ULK1 (Ser7575) relative to total ULK1 is significantly decreased in Sandhoff mice cerebellum (Fig. 1C). This indicates a decreased inhibition of ULK1 by mTORC1. mTOR, predominantly mTORC1, is phosphorylated and activated at Serine 2448 indirectly through the AKT pathway (Bostner et al., 2013). Western blots showed phospho-mTOR (Ser2448) relative to total mTOR was significantly decreased in Sandhoff mice cerebellum (Fig. 1D). These results indicate that mTORC1 is inhibited, and AMPK is active resulting in the induction of autophagy in the cerebellum of Sandhoff mice. Beclin-1 is also a key component of initiation of autophagy. However, relative expression of total Beclin-1 showed no significant difference in Sandhoff mice cerebellum (Fig. 1B).

A

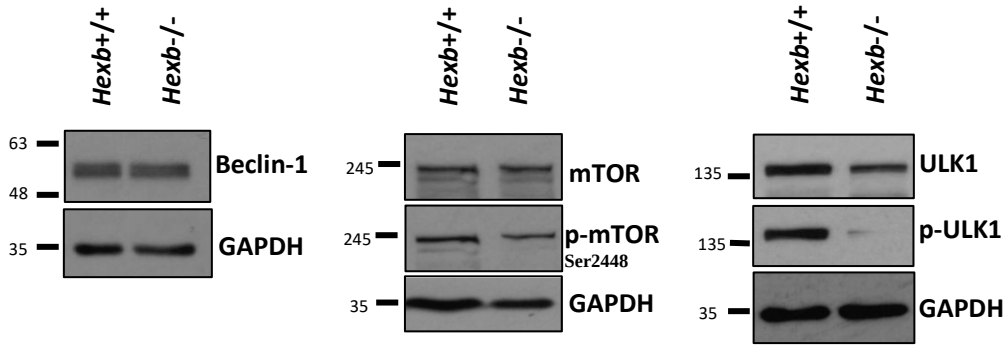
Hexb+/+
Hexb-/-
63
48
Beclin-1
35
GAPDH
245
mTOR
p-mTOR
Ser2448
135
ULK1
p-ULK1

B

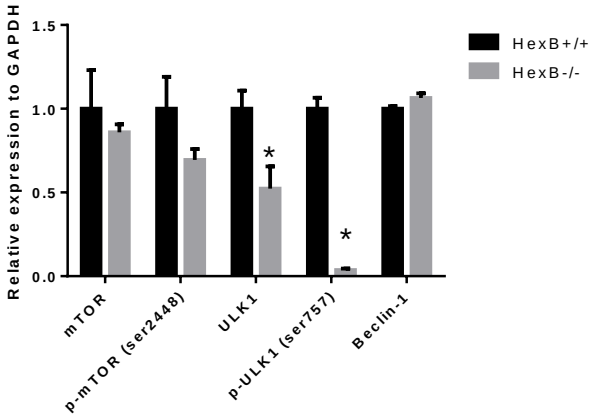
Relative expression to GAPDH
HexB+/+
HexB-/-
mTOR
p-mTOR (ser2448)
ULK1
p-ULK1 (ser757)
Beclin-1

C

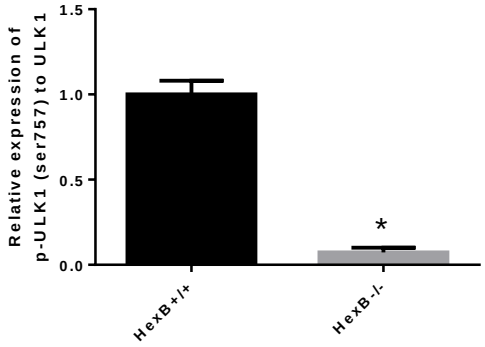
Relative expression of p-ULK1 (ser757) to ULK1
HexB+/+
HexB-/-

D

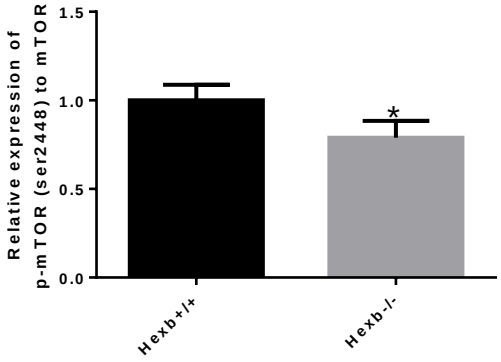
Relative expression of p-mTOR (ser2448) to mTOR
Hexb+/+
Hexb-/-

Figure 1. Autophagy is induced in the cerebellum of Sandhoff mice. Cerebellar lysates were retrieved from 120-day old Sandhoff (*Hexb*$^{-/-}$) and wild-type (*Hexb*$^{+/+}$) mice and analyzed using Western blots. A) Cerebellar lysates were blotted for Beclin-1, total mTOR, phospho-mTOR (ser2448), total ULK1, and phospho-ULK1 (ser757). Densitometry of the bands was measured using ImageJ and normalized against GAPDH to indicate protein expression levels. B) Expression of phospho-mTOR and total mTOR showed no change in Sandhoff mice compared to wild-type. Total Beclin-1 levels also remained unchanged. Phospho-ULK1 and total ULK1 expression relative to GAPDH were significantly decreased. C) Relative expression of phospho-ULK1 to total ULK1 is significantly decreased in Sandhoff mice. D) Relative expression of phospho-mTOR to total mTOR is significantly decreased in Sandhoff mice. These results indicate an initiation of autophagy in the cerebellum of Sandhoff mice.
Graphs represent average band intensity normalized to GAPDH. Data illustrates the mean ± SEM, n= 3.
*$P < 0.05$, Student's *t*-test.

3.2 Autophagy is blocked in Sandhoff mice cerebellum.

p62 was observed to accumulate in other LSDs and may be an indicator of impairment in the fusion of lysosomes with autophagosomes (Lieberman et al., 2012). Since p62 accumulation is appears to be an indicator of autophagic impairment, we sought to assess p62 levels in Sandhoff mice cerebellum. We hypothesized that p62 will be significantly increased in Sandhoff mice cerebellum, resulting in autophagic substrate accumulation. In order to investigate p62 levels in the cerebellum, western blot analysis was performed on cerebellum lysates from Sandhoff and wild-type mice. Results showed p62 expression relative to GAPDH was significantly increased in Sandhoff compared to the wild-type mice cerebellum (Fig. 2). This suggests an accumulation of p62 and a block of autophagic flux. This block of autophagic flux may result in unwanted cellular components remaining within the cell.

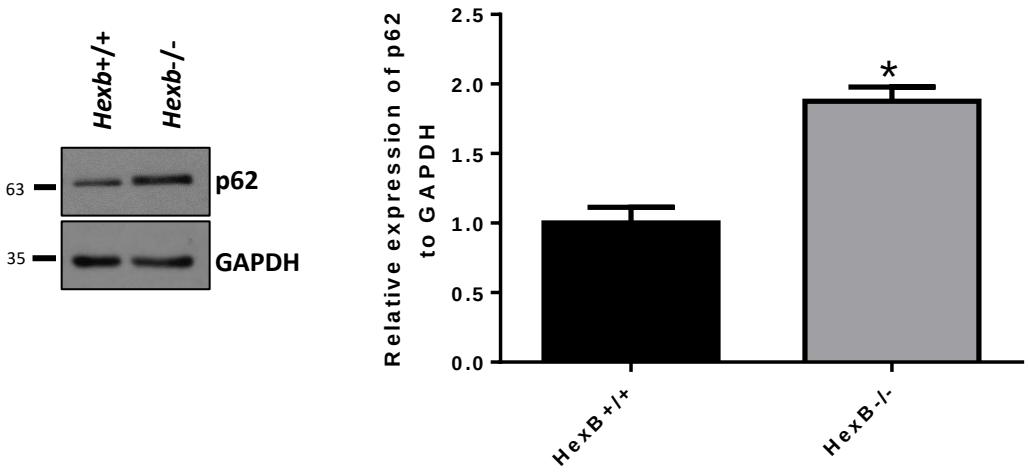

Figure 2. Autophagy is blocked in Sandhoff mice cerebellum. Cerebellar lysates were retrieved from 120-day old Sandhoff (*Hexb*$^{-/-}$) and wild-type (*Hexb*$^{+/+}$) mice and analyzed using Western blots. Cerebellar lysates were blotted for the autophagy markers p62, and TFEB. Densitometry of the bands were measured using ImageJ and normalized against GAPDH to indicate protein expression levels. Expression of p62 was significantly increased in *Hexb*$^{-/-}$ mice. P62 is an autophagy receptor protein responsible for delivering substrates to the autophagosome, where these substrates and p62 are degraded. An increase in p62 expression indicates an accumulation of the protein and an impairment in autophagic flux.
Graphs represent average band intensity normalized to GAPDH unless stated otherwise. Data illustrates the mean ± SEM, n= 3. *P < 0.05, Student's *t*-test.

3.3 Autophagy is induced in Sandhoff mice soleus muscle.

Next, we wanted to investigate autophagy within the muscles of LSD mouse models. Autophagy may be a pathway of interest for the muscle atrophy observed in LSD patients. Since we observed the induction of autophagy in the cerebellum of Sandhoff mice, we sought to elucidate whether a similar effect was observed in the soleus muscle. Soleus muscles have been previously observed for studies on muscle regeneration and myogenesis (Yusuf & Brand-Saberi, 2012). In fact, a study of a patient with an LSD revealed vacuolization and loss of myofibers in the soleus muscle (Prater, et al., 2013). Therefore, we analyzed the soleus muscle in order to elucidate the effect of LSDs on myogenic differentiation. We also utilized *Neu1*^{hypo} mice as a model for Sialidosis. However, it is important to note that *Neu1*^{hypo} mice are only sialidase mutants and do not have complete knockdown of Neu1. The model has been backcrossed 10 times with wild-type C57BL/6 mice.

Western blot analysis of autophagy markers phospho-ULK1, total ULK1, LC3, and mTOR was conducted on soleus muscle lysates from wild-type, Sandhoff and B10.SM mice to investigate levels of autophagy induction (Fig. 3A). No change was observed in the relative expression of phospho-mTOR (ser2448) and total mTOR to GAPDH in Sandhoff and *Neu1*^{hypo} mice when compared to the control (Fig. 3B). LC3-I and LC3-II showed no change in relative expression in Sandhoff and *Neu1*^{hypo} (Fig. 3B). However, the relative expression of phospho-mTOR to total mTOR was significantly decreased in Sandhoff mice and showed no change in *Neu1*^{hypo} mice (Fig. 3C). This indicates that mTOR is inactive in Sandhoff mice soleus muscle. Relative expression to GAPDH showed no change in total

ULK1; however, a significant decrease in phospho-ULK1 (ser757) and a significant increase phospho-ULK1 (ser555) expression was observed in Sandhoff mice compared to wild-type (Fig. 3D). Furthermore, the expression of phospho-ULK1 (ser757) was significantly decreased and the expression of phospho-ULK1 (ser555) was significantly increased relative to total ULK1 in Sandhoff mice (Fig. 3E). Similar to our observations within the cerebellum, these results suggest that mTOR is inactive and is unable to inhibit ULK1, while AMPK is activated and phosphorylates ULK1 to induce autophagy in Sandhoff mice soleus muscle.

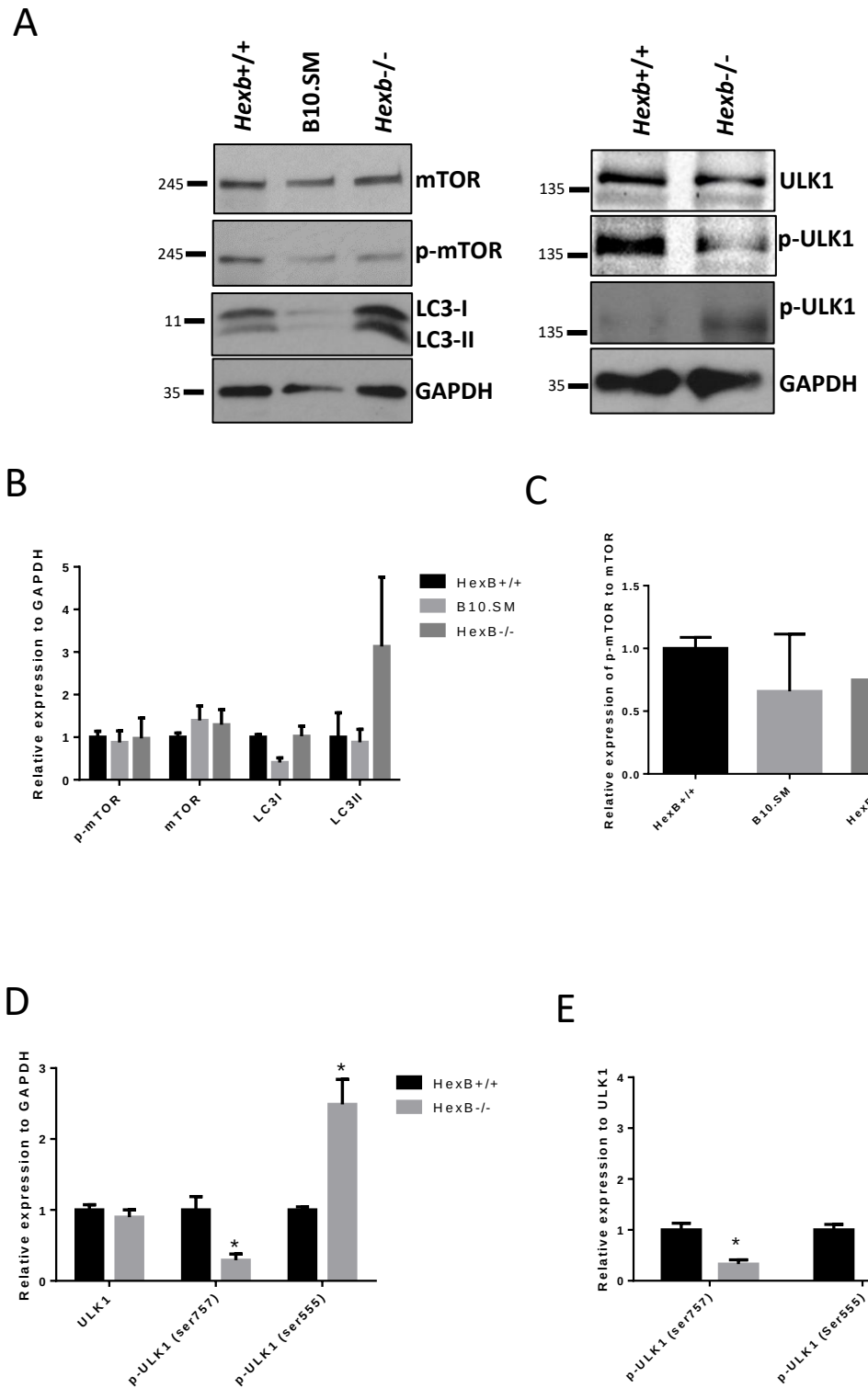
A
Hexb+/+
B10.SM
Hexb-/-
245
mTOR
245
p-mTOR
11
LC3-I
LC3-II
35
GAPDH
Hexb+/+
Hexb-/-
135
ULK1
135
p-ULK1
135
p-ULK1
35
GAPDH
B
Relative expression to GAPDH
HexB+/+
B10.SM
HexB-/-
p-mTOR
mTOR
LC3I
LC3II
C
Relative expression of p-mTOR to mTOR
HexB+/+
B10.SM
HexB-/-
D
Relative expression to GAPDH
HexB+/+
HexB-/-
ULK1
p-ULK1 (ser757)
p-ULK1 (ser555)
E
Relative expression to ULK1
HexB+/+
HexB-/-
p-ULK1 (ser757)
p-ULK1 (Ser555)

Figure 3. Autophagy is induced in the soleus muscle of Sandhoff mice. Soleus muscle lysates were retrieved from 120-day old Sandhoff (*Hexb*$^{-/-}$), B10.SM mice, and wild-type (*Hexb*$^{+/+}$) mice and analyzed using Western blots. A) Soleus muscle lysates were blotted for total mTOR, phospho-mTOR, LC3, total ULK1, phospho-ULK1 (ser757), and phospho-ULK1 (ser555). Densitometry of the bands were measured using ImageJ and normalized against GAPDH to indicate protein expression levels. B) Expression of phospho-mTOR and total mTOR showed no change in Sandhoff and B10.SM mice compared to wild-type. No change was also observed for LC3-I and LC3-II expression. C) The expression of phospho-mTOR to total mTOR showed a significant decrease in Sandhoff mice, but a significant change was not observed in B10.SM mice. This suggests an inactive mTOR. D) The expression of total-ULK1 was unchanged, phospho-ULK1 (ser757) significantly decreased, and phospho-ULK1 (ser555) significantly increased relative to GAPDH in Sandhoff mice compared to wild-type. E) Expression of phospho-ULK1 (ser757) was significantly decreased and phospho-ULK1 (ser555) was significantly increased relative to total ULK1 in Sandhoff mice. These results suggest an induction of autophagy in the soleus muscle of Sandhoff mice.
Graphs represent average band intensity normalized to GAPDH unless stated otherwise. Data illustrates the mean ± SEM, n= 3. *$P < 0.05$, Student's *t*-test.

3.4 Autophagy is blocked in Sandhoff mice soleus muscle.

Since p62 accumulation was observed in the cerebellum, we sought to elucidate whether a similar effect was observed in the soleus muscle. We wanted to determine whether an impairment of autophagy was also occurring in skeletal muscle tissue as this would present a possible cause of muscle dysfunction within LSD patients.

The relative expression of p62 in soleus muscle lysates from Sandhoff and wild-type mice was measured using western blot and band densitometry. Results showed p62 expression, relative to GAPDH, was significantly increased in Sandhoff compared to the wild-type mice (Fig. 4). This suggests an accumulation of p62 and a block of autophagy in the soleus muscle.

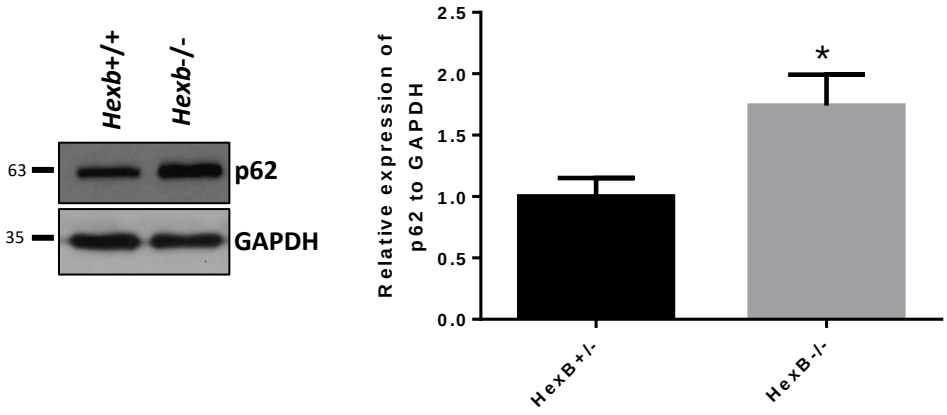

Figure 4. Autophagy is blocked in Sandhoff mice soleus muscle. Soleus muscle lysates were retrieved from 120-day old Sandhoff and wild-type mice and analyzed using western blots. The lysates were blotted for p62 protein expression. Densitometry of bands were measured using ImageJ and normalized against GAPDH. Expression of p62 is significantly increased in Sandhoff mice. An increase in p62 expression indicates an accumulation of the protein and a block of autophagic flux.
Graphs represent average band intensity normalized to GAPDH. Data illustrates the mean ± SEM, n= 3.
*P < 0.05, Student's *t*-test.

3.5 Myogenic Differentiation is Impaired in the Soleus Muscle of Sandhoff Mice.

Impairment in the process of myogenic differentiation as a result of altered autophagic flux may be the cause for muscle atrophy observed in LSD patients. Skeletal muscle degeneration has been observed in mouse models of LSDs such as Sialidosis (Zanoteli et al., 2010). In another study, an LSD mouse model showed autophagic accumulation in skeletal muscles (Lieberman et al., 2012). Furthermore, autophagy is a key regulator of skeletal muscle differentiation and basal levels are necessary for proper removal of unwanted proteins (Bonaldo and Sandri, 2013). Hence, we sought elucidate the impact of the induction of autophagy and a block in autophagic flux on myogenic differentiation in a mouse model for Sandhoff Disease.

To investigate the effects of LSDs on muscles and myogenic differentiation, soleus muscle lysates from Sandhoff, B10.SM and wild-type mice approximately 120 days of age were analyzed using western blot and blotted for the protein expression levels of myogenic differentiation markers. Myogenin is a muscle regulatory factor (MRF) which promotes differentiation through the fusion of myoblasts into myotubes in later stages of myogenesis. MHC is involved in the terminal stages of myogenesis (Champigny et al., 2005). Myogenin and MHC are necessary for terminal differentiation of myoblasts (Bharathy et al., 2013). Bands from the western blots were measured using the densitometry feature on ImageJ and normalized to GAPDH. The relative expression of myogenin and GAPDH significantly decreased in Sandhoff mice soleus muscle compared to wild-type (Fig.5). These findings indicate an impairment in myogenic differentiation in the soleus muscle of Sandhoff mice.

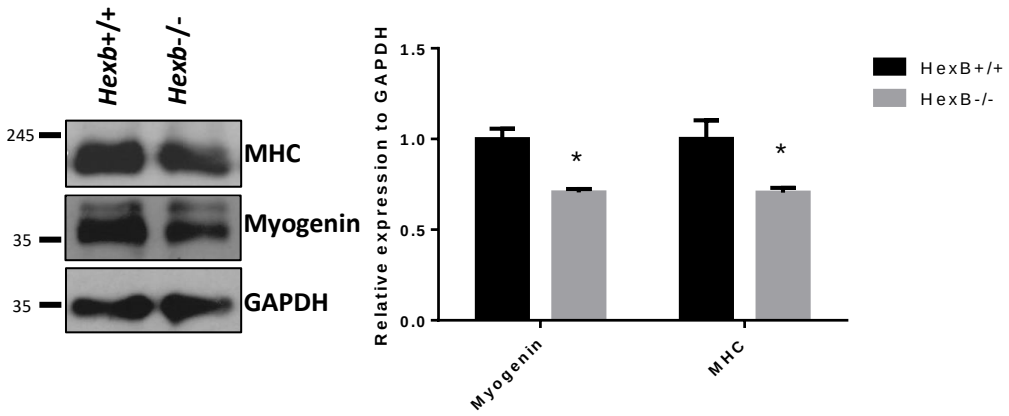

Figure 5. Myogenic differentiation was impaired in the soleus muscle of Sandhoff mice. Soleus muscle lysates were retrieved from 120-day old Sandhoff and wild-type mice and analyzed using western blots. The lysates were blotted for the myogenin and MHC. Densitometry of the bands were measured using ImageJ and normalized against GAPDH. Expression of myogenin and MHC were significantly decreased in the soleus muscle of Sandhoff mice compared to wild-type. These results suggest an impairment in the myogenic differentiation of myoblasts in Sandhoff mice. Graphs represent average band intensity normalized to GAPDH. Data illustrates the mean ± SEM, n= 3. *P < 0.05, Student's *t*-test.

3.6 Knockdown of lysosomal enzymes induced autophagy in differentiated C2C12 myoblasts.

An *in-vitro* model was used to extend the study on the impact of lysosomal enzyme deficiency and autophagy on myogenic differentiation. To investigate the effect of LSDs on autophagy in an *in-vitro* model, C2C12 mouse myoblasts were transfected with siRNAs to knockdown the lysosomal enzymes Neu1, *Hexb* and β-gal. These enzymes were knocked down to represent *in-vitro* models for Sialidosis, Sandhoff Disease, and GM1-gangliosidosis respectively. C2C12 myoblasts were used in order to determine if a similar effect on autophagy and myogenesis was observed at the cellular level as our *in-vivo* mouse models. Furthermore, it should eliminate other confounding variables that may be contributing within the mouse models and further isolate autophagy as a possible pathway of interest. The use of myoblast cells should determine the impact of lysosomal enzyme deficiency on muscles at a cellular level, and to differentiate this impact from the physiological effect of neurodegeneration on muscle tissue. Previous studies have shown that alterations to the expression levels of lysosomal enzymes have resulted in inhibition of myogenesis. Overexpression of Neu1 in C2C12 myoblasts inhibited myoblast fusion and myogenic differentiation (Champigny et al., 2005). The C2C12 cell line was a good model of mouse myoblasts since it expresses characteristic muscle markers upon differentiation and has several advantages over primary myoblasts, namely greater accessibility and homogeneity (Champigny et al., 2005).

C2C12 myoblasts were transfected with siRNA to knockdown Neu1, *Hexb*, and β-gal for 24h (treatment cells). The control cells were transfected with negative control siRNA. The cells were then incubated in differentiation media and allowed to differentiate

into multi-nucleated myotubes for 120h. After 120h, the differentiated myotubes were terminated and lysed. Cell lysates were run on SDS-Page and analyzed by western blots for autophagy markers (Fig. 6A). Neu1 expression levels were also measured to verify that the siRNA knockdowns were successful. Protein expression levels were determined by measuring the densitometry of the bands produced from the western blots. Neu1 expression, relative to GAPDH, was significantly decreased in the cells treated with siRNA for Neu1 compared to those treated with the negative control, siRNA for *Hexb* and siRNA for β-gal (Fig. 6B). This indicates that the siRNA transfections were successful in knocking down our specific lysosomal enzymes of interest. Knockdown of Neu1, *Hexb*, and β-gal significantly decreased expression of phospho-ULK1 (ser757) relative to total ULK1 (Fig. 6C). On the other hand, the expression of phospho-ULK1 (ser555) to total ULK1 was significantly increased (Fig. 6C). These results suggest that mTORC1 is inhibited and was unable to phosphorylate ULK1, while AMPK is activated and phosphorylated ULK1 to induce autophagy. Knockdown of the lysosomal enzymes involved in LSDs induces induction of autophagy in C2C12 myoblasts.

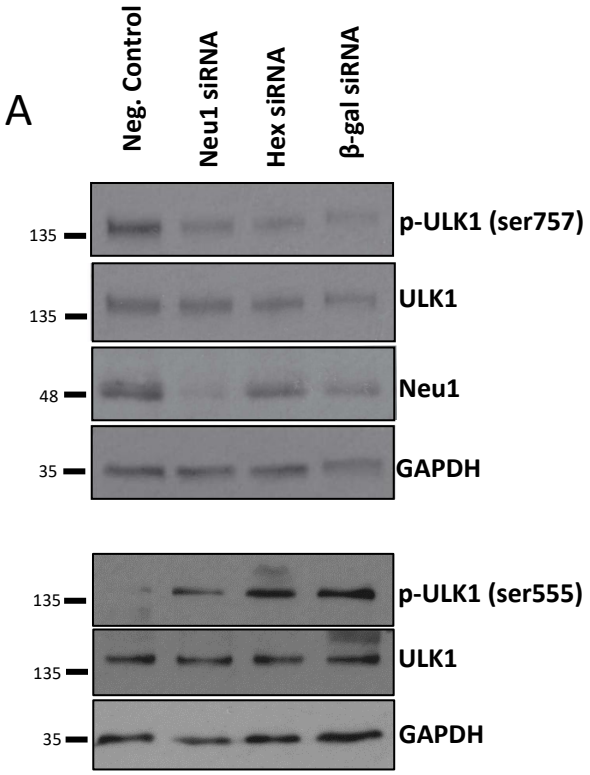
A
Neg. Control
Neu1 siRNA
Hex siRNA
β-gal siRNA
135
p-ULK1 (ser757)
135
ULK1
48
Neu1
35
GAPDH
135
p-ULK1 (ser555)
135
ULK1
35
GAPDH

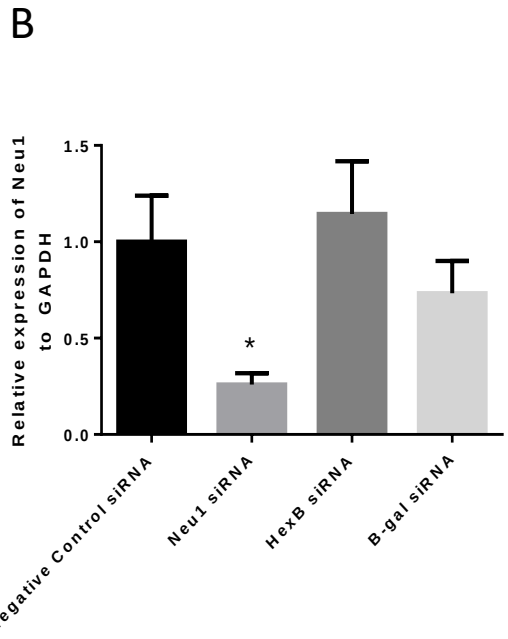
B
Relative expression of Neu1 to GAPDH
1.5
1.0
0.5
0.0
*
Negative Control siRNA
Neu1 siRNA
HexB siRNA
B-gal siRNA

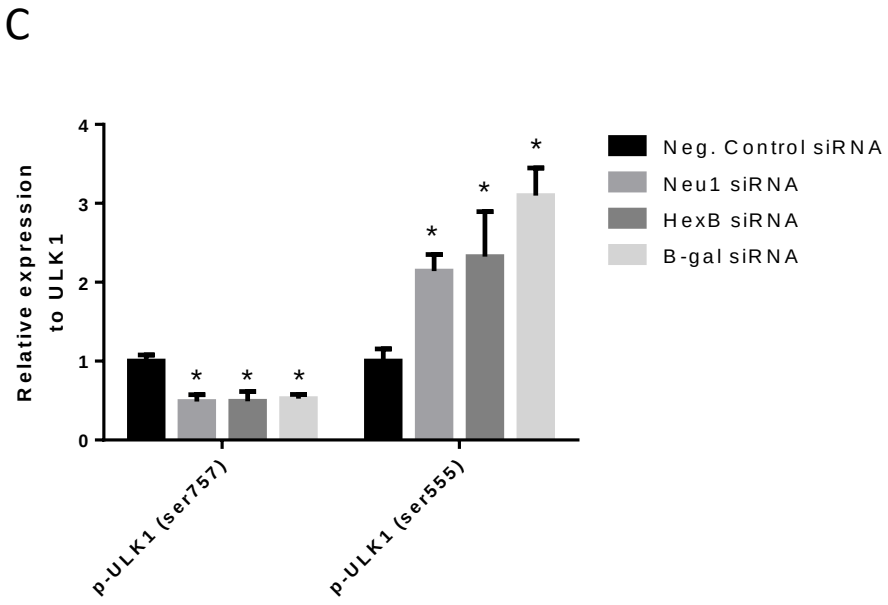
C
Relative expression to ULK1
4
3
2
1
0
*
*
*
*
*
*
p-ULK1 (ser757)
p-ULK1 (ser555)
Neg. Control siRNA
Neu1 siRNA
HexB siRNA
B-gal siRNA

Figure 6. siRNA knockdowns of lysosomal enzymes induced autophagy in differentiated C2C12 myoblasts. C2C12 myoblasts were transfected with siRNAs to knockdown Neu1, *Hexb*, β-gal for 24h and differentiated into multinucleated myotubes for 120h. The cell lysates were analyzed for protein expression levels using Western blots. A) The lysates were western blotted for autophagy markers. Densitometry of the bands was measured using ImageJ and normalized against GAPDH. B) Neu1 was significantly decreased in the cells treated with Neu1 knockdown, indicating that that siRNA transfections were successful. C) Expression of phospho-ULK1 (ser757) was significantly decreased and phospho-ULK1 (ser555) was significantly increased relative to total ULK1 in cells transfected with siRNA for Neu1, *Hexb*, and β-gal compared to cells transfected with negative control siRNA. These results indicate that autophagy is induced during knockdown of the lysosomal enzymes Neu1, *Hexb* and β-gal in C2C12 myotubes.
Graphs represent average band intensity. Data illustrates the mean ± SEM, n= 4. *$P < 0.05$, One-way Anova.

3.7 Knockdown of lysosomal enzymes induced a block in autophagy in differentiated C2C12 myoblasts.

LSD cells have shown impairment in the process of autophagic flux as evident by the accumulation of p62 (Igdoura, unpublished and others). Since a block of autophagic flux was observed in our *in-vivo* mouse model of LSDs, we sought to elucidate whether a similar effect was occurring in our *in-vitro* cell models of LSDs. In order to do this, we observed the expression levels of the autophagic substrate, p62. Cell lysates from the siRNA-transfected and differentiated C2C12 myoblasts were western blotted for p62. Expression of p62 was significantly increased in the treatment cells compared to the negative control. (Fig. 7). Since p62 is normally observed to significantly decrease as myogenic differentiation of C2C12 progresses, this indicates an accumulation of the autophagic substrate p62 and a block in autophagic flux due to a deficiency of lysosomal enzymes (McMillan and Quadrilatero, 2014).

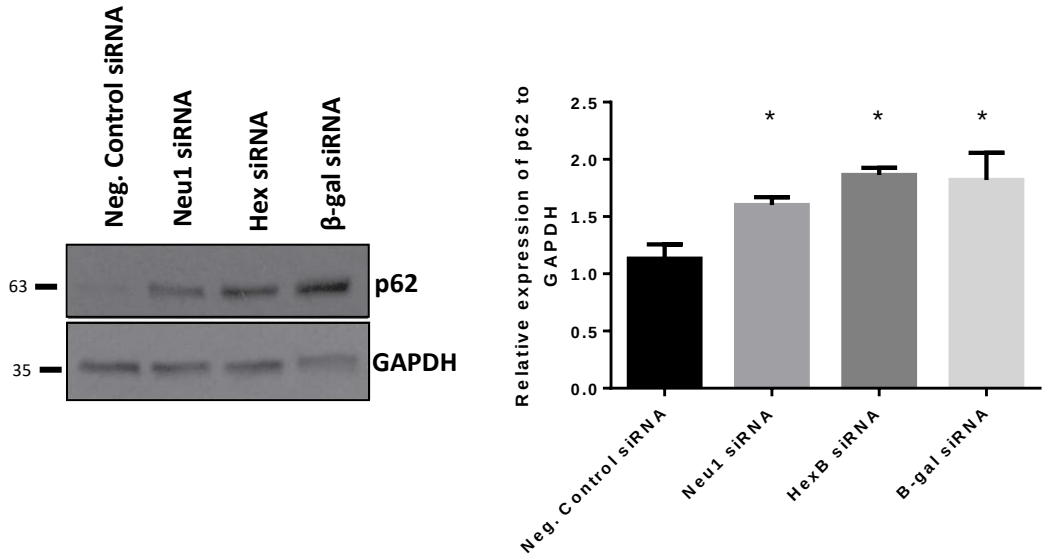

Figure 7. siRNA knockdowns of lysosomal enzymes induced a block autophagy in differentiated C2C12 myoblasts. C2C12 myoblasts were transfected with siRNAs to knockdown Neu1, *Hexb*, β-gal for 24h and differentiated into multinucleated myotubes for 120h. The cell lysates were western blotted for the autophagic substrate, p62. Densitometry of the bands was measured using ImageJ and normalized against GAPDH. Expression of p62, relative to GAPDH, was significantly increased in cells transfected with siRNA for Neu1, *Hexb*, and β-gal compared to those transfected with negative control siRNA. These results indicate a block in autophagic flux.
Graphs represent average band intensity. Data illustrates the mean ± SEM, n= 4. *P < 0.05, One-way Anova.

3.8 Knockdown of lysosomal enzymes inhibited cell fusion and myogenic differentiation of C2C12 myoblasts.

Since autophagy is essential during myogenic differentiation, and inhibition of autophagy prevents proper differentiation and fusion in C2C12 myoblast cells, we wanted to elucidate how the block in autophagic flux that was observed in our siRNA-treated myoblasts would impact fusion and myogenic differentiation (Fortini et al., 2016). We sought to quantitatively measure myoblast fusion and differentiation through protein expression levels of myogenin and MHC. To do this, cell lysates from siRNA-treated and differentiated C2C12 were run on SDS-Page and analyzed by western blots for myogenic differentiation markers. Expression of myogenin and MHC was significantly decreased in the treatment cells compared to the negative control cells (Fig. 8). This indicates that a deficiency of the lysosomal enzymes Neu1, *Hexb* and β-gal inhibits expression of MRFs necessary for the terminal stages of myogenesis.

The ability of siRNA transfected cells to undergo fusion and form myotubes was also measured using a differentiation index from cell counting. At 24h, 48h, and 72h after the initiation of differentiation, phase contrast images of the transfected cells were taken under an inverted microscope. Each of the siRNA treatments and control cells were imaged for 20 random areas under 400x magnification and the number of cells as well as the number of nuclei within each cell was counted for every area. In order to extrapolate the number of myotubes for each plate, the area observed under the 200x magnification was extrapolated to the area of the plate (2.8 x 109 μm2) (Fig. 9). At 24h, our negative control cells had significantly more myotubes with 2 – 3 and 4 – 6 nuclei than our treatment cells (Fig. 9A). At 48h, our negative control cells had significantly more myotubes with 16 – 9

nuclei compared to our treatment cells (Fig. 9B). At 72h, our negative control cells had significantly more myotubes containing greater than 26 nuclei compared to our treatment cells (Fig. 9C). From 24h to 72h post-differentiation, our negative control cells favoured the formation of myotubes containing increasingly greater numbers of nuclei. However, in our treatment cells the formation of myotubes with many nuclei was significantly impaired and the increase in nuclei within each myotube was delayed from 24h to 72h.

Prior to termination at 120h of differentiation, phase contrast images of the transfected cells were also taken. Each of the siRNA treatments and control cells were imaged for 20 random areas under 400x magnification and the number of cells as well as the number of nuclei within each cell was counted for every area. Images of the negative control siRNA-treated cells showed many multinucleated myotubes, which appear as elongated and large tube-like structures with many nuclei (Fig. 10A). Images of cells with knockdown of lysosomal enzymes showed some elongation of myoblasts; however, there appeared to be much less multinucleated myotubes (Figs. 10B, C, D). Some myotubes formed but were much smaller and contained less nuclei. The differentiation index was calculated as the proportion of multinucleated cells over the total number of cells in each image. It was observed that the percentage of multinucleated myotubes was significantly decreased in the treatment cells compared to the negative control cells (Fig. 10E).

To produce sharper and distinct qualitative images to portray the effect of lysosomal enzyme knockdown on myogenic differentiation, immunocytochemistry experiments were conducted on siRNA-treated cells. The images were used to portray the localization of myogenin, MHC and nuclei as a way to visualize myoblast fusion and differentiation. Prior

to transfection and differentiation, C2C12 myoblasts were cultured onto glass coverslips. The cells were then transfected and differentiated for 120h. The cells were fixed and were scored immunocytochemically with antibodies for myogenin, and MHC and were doubly stained with DAPI for staining of nuclei. The cells were transferred onto slides and imaged under the 40x lens of a fluorescence microscope (Zeiss, Axiovert200). Fluorescent images of cells doubly stained with myogenin and DAPI revealed several long myogenin-positive myotubes with many nuclei in the negative-control cells (Fig. 11). However, for the cells transfected with siRNA to knockdown specific lysosomal enzymes, very few, if any, myogenin-positive myotubes were evident. The myotubes that can be observed appeared to be visibly smaller and contained less nuclei than the myotubes in the negative control cells (Fig. 10). Cells stained with MHC and DAPI showed similar results (Fig. 12). In the negative control cells, large MHC-positive myotubes with many nuclei (>20) were observed. In the siRNA-treatment cells, some elongated MHC-positive myotubes are observed; however, they are considerably smaller and contain less nuclei than those in the negative controls (Fig. 12).

The western blot analysis, phase contrast images and cell counting differentiation index, and the immunocytochemistry images indicate that C2C12 myoblasts with knockdown of Neu1, *Hexb* and β-gal have a reduced ability to undergo myogenic differentiation. Cells with knockdown of these lysosomal enzymes regularly had less myotube formation and the myotubes which did form were visibly smaller and contained less nuclei. This suggests that the ability of myoblasts to recruit and fuse with other myoblasts was significantly impaired.

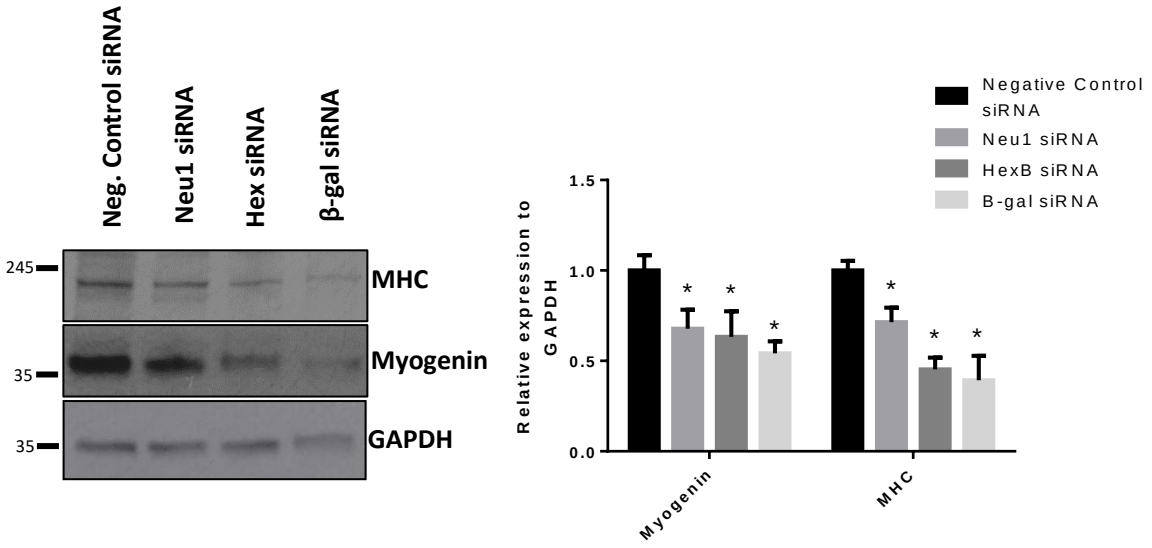

Figure 8. Knockdown of lysosomal enzymes inhibits expression of MRFs essential to myogenic differentiation. C2C12 myoblasts were transfected with siRNAs to knockdown Neu1, *Hexb*, β-gal for 24h and differentiated into multinucleated myotubes for 120h. The cell lysates were western blotted for myoblast fusion and terminal differentiation markers, myogenin and MHC. Densitometry of the bands was measured using ImageJ and normalized against GAPDH. Myogenin and MHC expression showed a significant decrease in the treatment cells compared to the negative control. These results indicate that knockdown of lysosomal enzymes result in reduced myoblast fusion and differentiation in C2C12 myoblasts.
Graphs represent average band intensity. Data illustrates the mean ± SEM, n= 4. *P < 0.05,
One-way Anova.

A) 24h post-differentiation

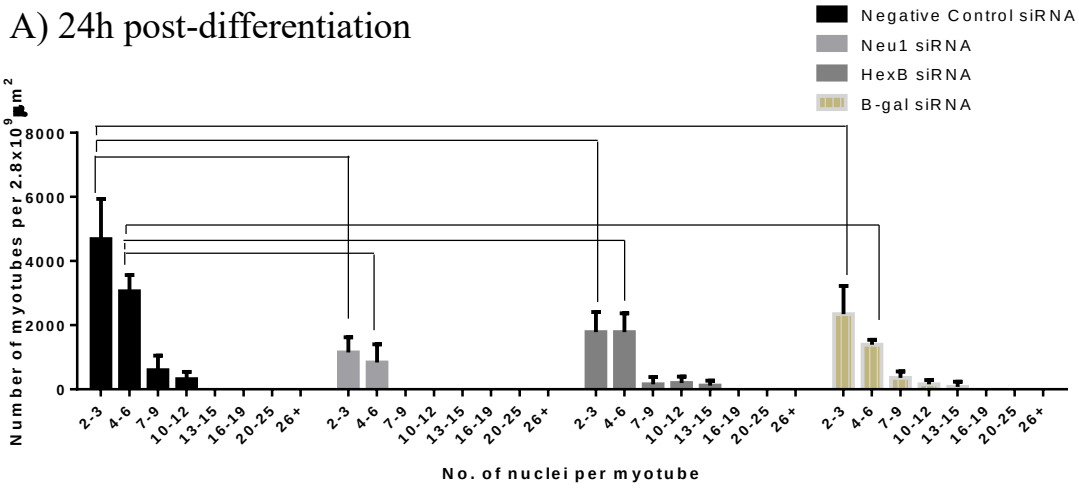

B) 48h post-differentiation

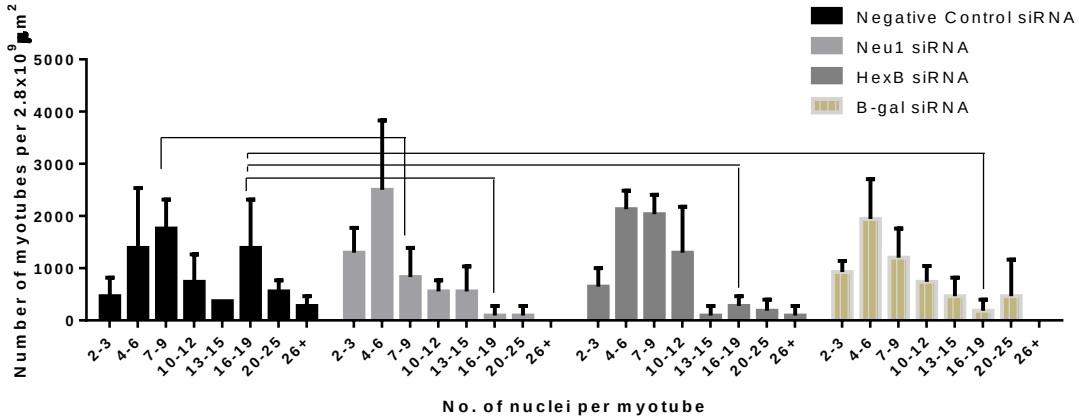

C) 72h post-differentiation

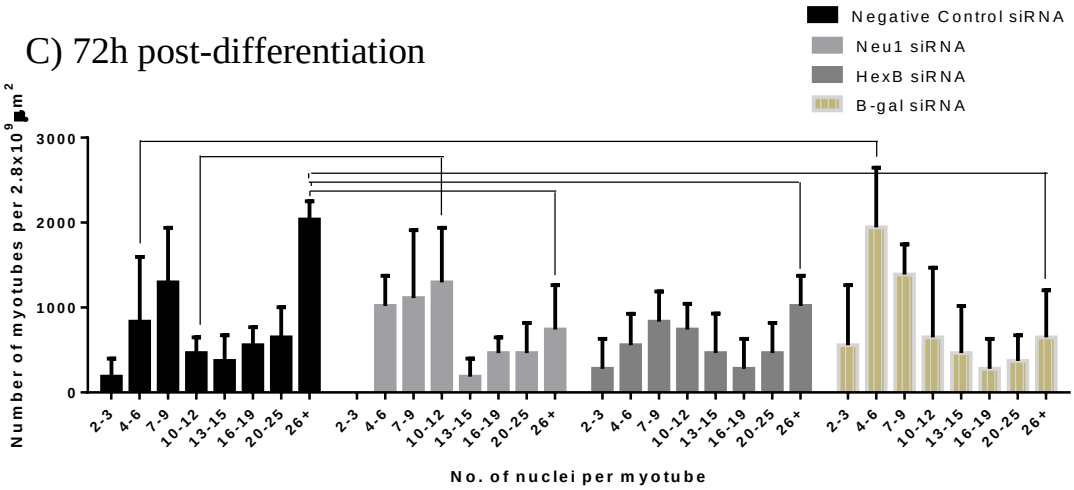

Figure 9. Knockdown of lysosomal enzymes delays and impairs formation of multinucleated myotubes. C2C12 myoblasts were transfected with siRNAs to knockdown Neu1, *Hexb*, β-gal for 24h and differentiated into multinucleated myotubes for 120h. At the 24h, 48h and 72h post-differentiation, 8 random areas for each plate was observed and the number of myotubes (C2C12 cells with more than 1 nucleus) was counted at 200x magnification on an inverted microscope. In order to extrapolate the number of myotubes for each plate, the area observed under the 200x magnification was extrapolated to the area of the plate (2.8×10^9 μm^2). A) At 24h, our negative control cells had significantly more myotubes with 2 – 3 and 4 – 6 nuclei than our treatment cells. B) At 48h, our negative control cells had significantly more myotubes with 16 – 9 nuclei compared to our treatment cells. C) At 72h, our negative control cells had significantly more myotubes containing greater than 26 nuclei compared to our treatment cells. This indicates an impairment in the ability of nascent myoblasts to recruit and fuse with other myoblasts to form multinucleated myotubes.

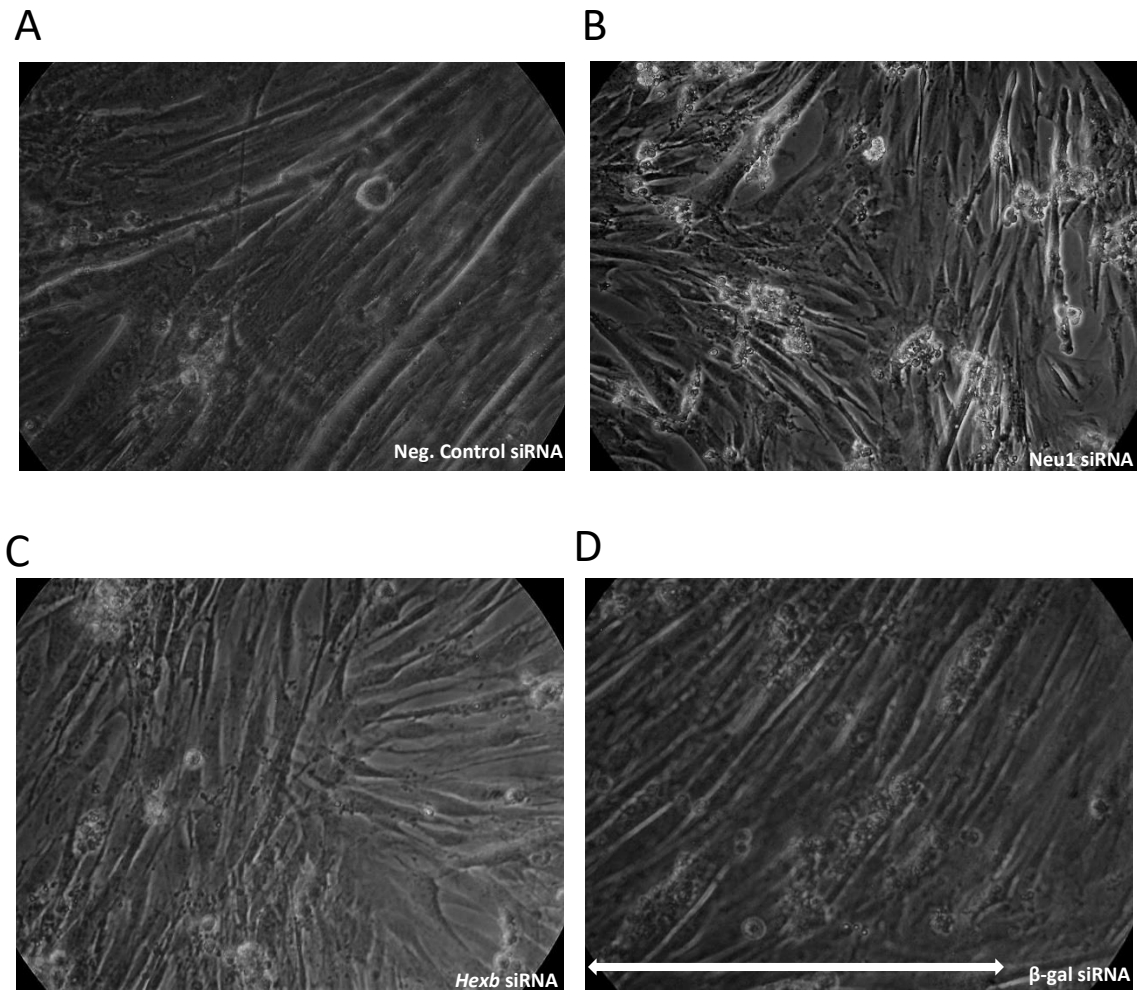
A
B
Neg. Control siRNA
Neu1 siRNA
C
D
Hexb siRNA
β-gal siRNA
E
Percentage of multinucleated myotubes
0.0
0.2
0.4
0.6
0.8
*
*
*
Negative Control
Neu1
HexB
Beta-gal

Figure 10. Knockdown of lysosomal enzymes inhibits fusion of myoblasts and results in smaller myotubes with fewer nuclei. C2C12 myoblasts were transfected with siRNAs to knockdown Neu1, *Hexb*, β-gal for 24h and differentiated into multinucleated myotubes for 120h. Phase contrast images of the transfected cells were taken under an inverted microscope. Each of the siRNA treatments were imaged for 20 random areas under 400x magnification and the number of cells as well as the number of nuclei within each cell was counted for every area. A) Large myotubes with many nuclei are observed. Majority of the cells appear tubular, suggesting that a high percentage of them have differentiated into myotubes. B) Very little myotube formation, majority of the cells appeared to contain a single nucleus, while some have 2 to 3. C) Very few myotube formation, majority of the cells appeared to contain a single nucleus. D) Some myotube formation is visible; however, the myotubes were smaller and contained few nuclei. Scale bar represents 3µm. E) The differentiation index was calculated as the percentage of multinucleated cells over the total number of cells in each image. The proportion of multinucleated myotubes was significantly decreased in the siRNA-treatment cells after 120h of differentiation.
Graphs represent average band intensity. Data illustrates the mean ± SEM. *$P < 0.05$, One-way Anova.

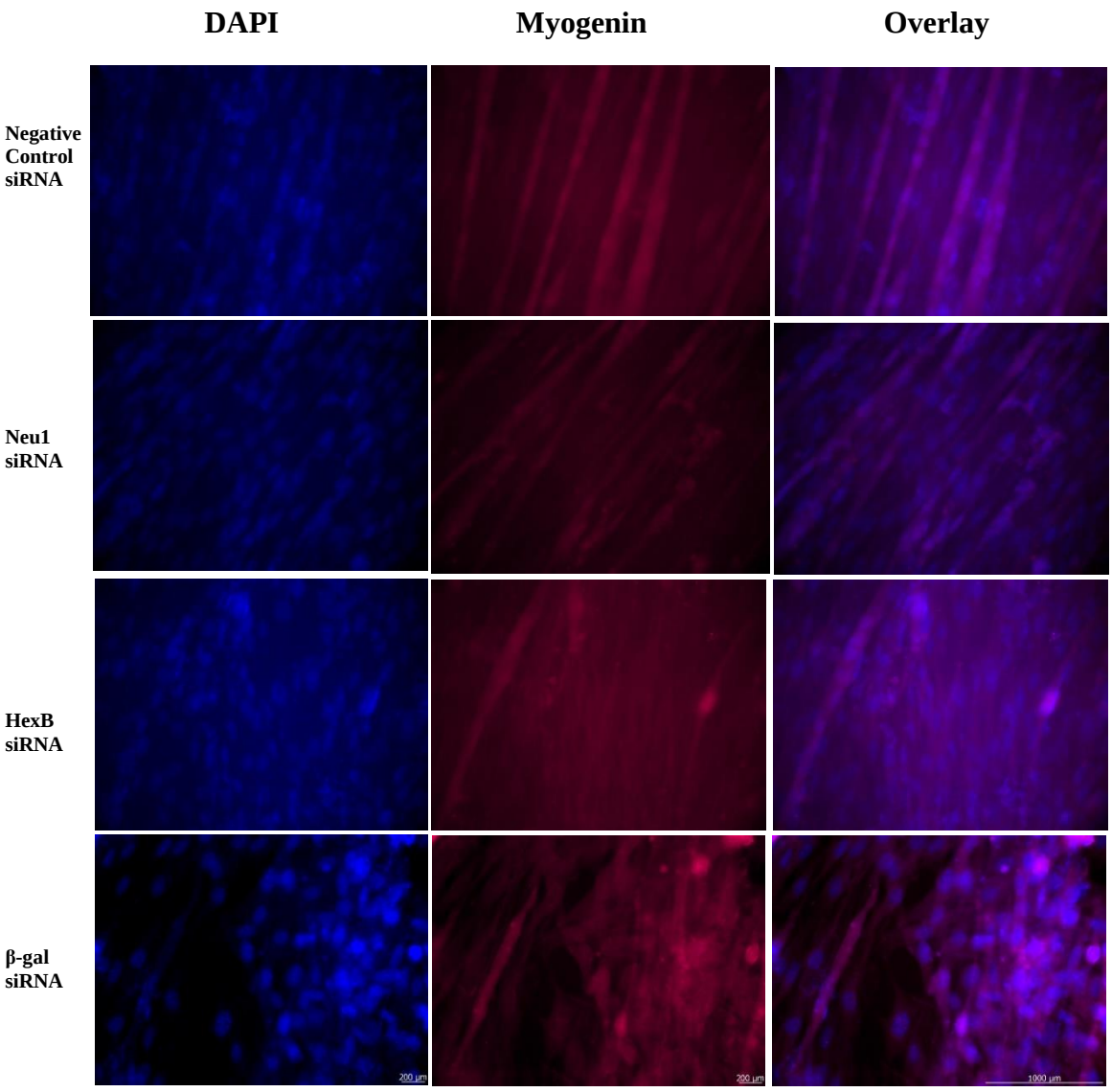

Figure 11. Knockdown of lysosomal enzymes impaired myotube formation. C2C12 myoblasts were transfected with siRNAs to knockdown Neu1, *Hexb*, β-gal for 24h and differentiated into multinucleated myotubes for 120h. Differentiation was assessed immunocytochemically after 120h. Cells were doubly stained with anti-myogenin and DAPI for nuclear DNA. Cells treated with siRNA for Neu1, *Hexb* and β-gal, showed visibly reduced myogenin-positive myotubes compared to the negative control cells. This indicates that knockdown of lysosomal enzymes reduced the ability of myoblasts to undergo myogenesis.
Scale bars represent 1000µm.

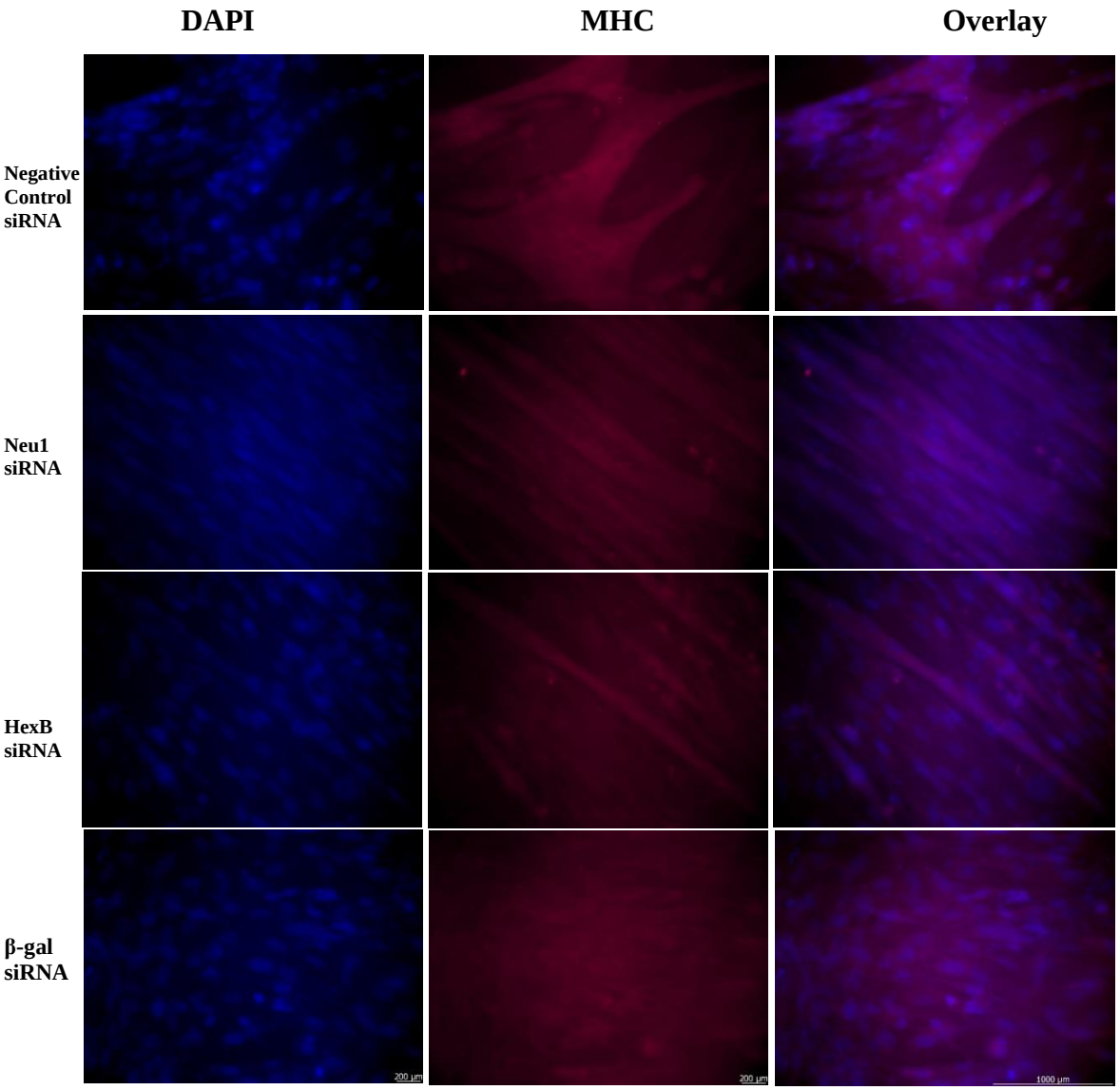

Figure 12. Knockdown of lysosomal enzymes favoured smaller myotubes with fewer nuclei. C2C12 myoblasts were transfected with siRNAs to knockdown Neu1, *Hexb*, β-gal for 24h and differentiated into multinucleated myotubes for 120h. Cells were doubly stained with anti-MHC and DAPI for nuclear DNA. Cells treated with siRNA for Neu1, *Hexb* and β-gal, showed visibly reduced MHC-positive myotubes compared to the negative control cells. Furthermore, myotubes in the lysosomal enzyme knockdown cells showed smaller myotubes with fewer nuclei. This indicates that knockdown of lysosomal enzymes reduced the ability of myoblasts to undergo myogenesis. Scale bars represent 1000µm.

Chapter 4: Discussion

In this study, we assessed the impact of lysosomal storage disorders on autophagy and myogenic differentiation. We wanted to investigate the processes of autophagy and myogenic differentiation as possible targets for alleviation of muscle dysfunction observed in LSDs. Autophagy is essential to a number of processes within the cell and has been observed to play a crucial role in myogenic differentiation (Fortini et al., 2016). It is necessary for myoblast remodelling and elimination of unwanted structures such mitochondria during the fusion of myoblasts (Fortini et al., 2016). Inhibition of autophagy in muscle cells have been observed to impair myogenesis. Knockdown of Beclin-1 in C2C12 cells reduced myoblast fusion significantly (Fortini et al., 2016). Hence, we investigated the state of autophagy using an *in-vivo* and *in-vitro* model for LSDs. We harvested cerebellum and soleus muscle tissues from Sandhoff mice, in which the *Hexb* gene was knocked out, and B10.SM mice, which were sialidase mutants backcrossed 10 times with C57BL/6 wild-type mice. We also knocked down specific lysosomal hydrolases within C2C12 myoblasts and differentiated them into myotubes. Mouse cerebellum and soleus muscle, and C2C12 lysates were then analyzed using western blot and immunocytochemistry.

Autophagy Induction in LSDs

Western blot analysis of Sandhoff mice cerebellum and soleus muscle revealed that autophagy was induced when compared to wild-type mice (Figs. 1 & 3). In Sandhoff mice, expression of phospho-mTOR (ser2448) over total mTOR was significantly decreased compared to wild-type mice. Phospho-ULK1 (ser757) was significantly increased and

phospho-ULK1 (ser555) was decreased relative to total ULK1. These results indicate that mTOR is inhibited, while AMPK is activated. AMPK then phosphorylates and activates ULK1, which initiates autophagy by phosphorylating a complex consisting of VPS34 and Beclin-1 (Fig. 13). Since basal levels of autophagy are required for normal cell function, these results do not suggest that autophagy is completely inhibited in wild-type mice and activated in Sandhoff mice, rather they indicate that autophagy induction is upregulated past basal levels in Sandhoff mice. This is in agreement with previous studies which presented an induction of autophagy in mouse models of other LSDs. The brain of GM1-gangliosidosis mouse models depicted increased levels of LC3-II indicating induction of autophagy (Takamura et al., 2008). Autophagy markers showed no change in expression levels in B10.SM mice. This may be because the mice are only sialidase mutants, and do not have complete knockout of the gene. Residual activity of Neu1 within these mice may be enough to prevent autophagic impairment. Furthermore, they have been backcrossed 10 times with wild-type C57BL/6 mice, and show no neurodegenerative phenotype as they age, unlike the Sandhoff mice.

A function of autophagy is to maintain cellular energy when a cell experiences different forms of stress (Takamura et al., 2008). Hence, the induction of autophagy may be due to the stress experienced by the cells as a result of lysosomal enzyme deficiency. In the cerebellum, the degeneration of neuronal cells may result in this induction of autophagy. It is possible that this neurodegeneration experienced by Sandhoff mice may be inducing cascading physiological effects into the soleus muscles. However, it is also possible that

the muscles cells themselves are affected by the deficiency of the *Hexb* gene, causing in induction of autophagy.

In order to determine whether this induction of autophagy is caused at a cellular level rather than a physiological one, we knocked down specific lysosomal enzymes in C2C12 myoblasts as *in-vitro* models for Sialidosis, Sandhoff disease and GM-1 gangliosidosis. We also wanted to extend the study on the impact of LSDs on autophagy and myogenic differentiation. siRNA-knockdown of Neu1, *Hexb*, and β-gal resulted in an induction of autophagy in differentiated C2C12 myoblasts. Phospho-ULK1 (ser757) was significantly increased and phospho-ULK1 (ser555) decreased relative to total ULK1 in the knockdown cells compared to the negative control cells (Fig. 6). In support of the results from our mouse models, these results indicate that mTOR is inhibited, and AMPK is activated, thereby allowing it to induce the initiation of autophagy through ULK1. Thus, our observations demonstrate an impact of the knockdown of lysosomal enzymes on muscles at a cellular level.

Block of Autophagy in LSDs

Western blot analysis of lysates from our *in-vivo* and *in-vitro* models of LSDs showed a significant increase of p62 expression (Figs. 2, 4 & 7). These results indicate an accumulation of p62 and a block of autophagic flux since p62 is normally degraded as autophagy progresses. Considering p62 is tagged onto unwanted substrates which are to be degraded in autophagy, an accumulation of p62 also indicates an accumulation of undegraded substrates, which can be toxic to the cell (Fig. 13). These substrates can include

aberrant mitochondria, which can release proapoptotic factors and reactive oxygen species, and oligomerized ubiquitin-positive aggregates, which are toxic to organelles (Sandri, 2010). Our results are in agreement with previous studies which observed p62 accumulation in other LSDs. An accumulation of p62 was observed in the skeletal muscle of a mouse model for an LSD called Pompe disease (Lieberman et al., 2012).

This accumulation of p62 may be due to the inability of the autophagosome to fuse with the lysosome and form an autophagosome, where the unwanted substrates are degraded. Observations from previous studies suggest a similar condition occurring in other LSDs. For example, in-vitro experiments for mucolipidosis II and III observed an increase in levels of autophagosomes in fibroblasts, which may indicate a defect in their ability to fuse with lysosomes (Otomo et al., 2009). Cells from mouse models of two LSDs showed accumulation of p62 and decreased co-localization between autophagosomes and lysosomes, indicating that this block of autophagy was due to a defect in fusion (Ballabio and Gieselmann, 2009). This supports the hypothesis that lysosomal storage disorders affect the ability of the lysosome to contribute to autophagy. This defect in fusion may be due to the accumulation of undegraded glycosides within the lysosome in LSDs. If the autophagosome, containing the substrates labelled with p62, is unable fuse with a lysosome, then autophagy cannot progress and autophagic substrates may begin to accumulate. Nevertheless, it is also feasible that fusion of autophagosomes with lysosomes does occur, but there is an impairment in the ability of the autophagolysosome to degrade the substrates due to a deficiency of specific lysosomal enzymes or the ability of cell to clear these

autophagolysosomes once autophagy has been completed. In other LSDs, fibroblasts showed a decreased ability to clear autophagolysosomes (Otomo et al., 2009).

A third possibility is that dysfunction upstream of p62 in the autophagic pathway caused this accumulation of autophagic substrates. Impairments in the development and maturation of nascent autophagosomes may lead to complications downstream in the process of autophagy, which could result in the inability of autophagosomes to fuse with lysosomes or the decreased ability of cells to clear autophagolysosomes. In one LSD mouse model, the accumulation of autophagic vacuoles was only observed in early autophagosomes, suggesting an impairment in the maturation step (Tanaka et al., 2000). Autophagosomes were unable to mature into late autophagosomes, and instead accumulated as vacuoles in the skeletal muscle and other tissues of the mice (Tanaka et al., 2000). Reduced clearance of autophagosome vacuoles can be fatal to the cell (Parkinson-Lawrence et al., 2010).

Some LSD's have shown an induction of autophagy, while others have shown a block of autophagy, with both resulting in the accumulation of autophagic substrates (Ballabio and Gieselmann, 2009). A theory has been suggested that a defect in the fusion of autophagosomes and lysosomes leads to an incomplete block of autophagy. A negative feedback loop to compensate for this block of autophagy is the upregulation of autophagic induction (Fig. 15). This further upregulation of autophagy could exacerbate the accumulation of unwanted substrates and autophagic vacuoles, which are toxic to the cell.

This induction of autophagy and block of autophagic flux results in a variety of consequences for the cell and may contribute to the muscle dysfunction observe in LSDs

(Fig. 15). One such consequence is the accumulation of abnormal mitochondria resulting in mitochondrial impairment (Sandri, 2010). Although induced autophagy is the cell's response to various types of stress, an upregulation of autophagy can lead to an abnormal overproduction of autophagosomes, which can be toxic to the cell as they aggregate into vacuoles (Ballabio and Gieselmann, 2009). Suppression of autophagy in mice were observed to cause build-up of ubiquinated protein aggregates, induce oxidative stress and negatively impact DNA stability, all of which led to myofiber degeneration (Sandri, 2010). Furthermore, accumulation of these toxic autophagic substrates often lead to an inflammatory response from cell, resulting in further cellular stress and damage (Ballabio and Gieselmann, 2009).

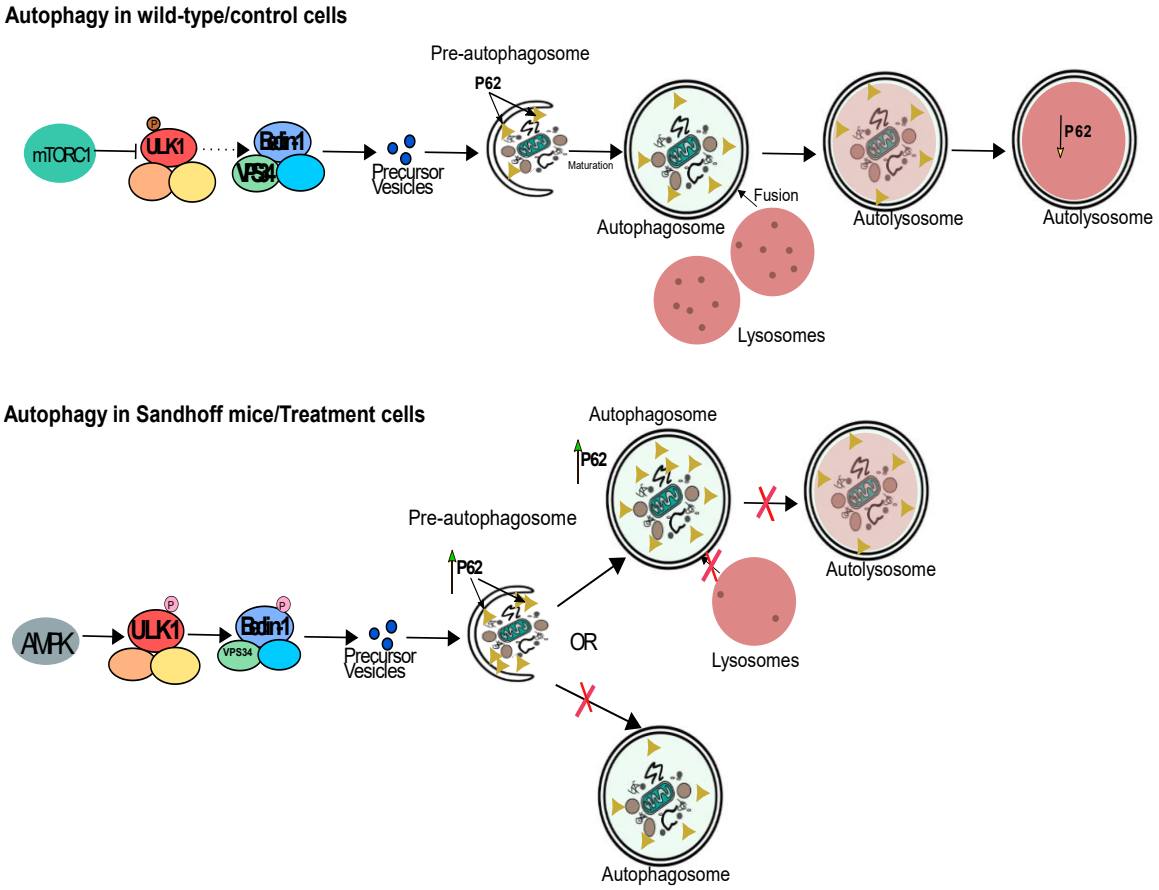

Figure 13. Autophagy is induced and blocked in LSD mouse and cell models. A) In wild-type (*Hexb*$^{+/+}$) mice and C2C12 myoblasts transfected with negative control siRNA, autophagy is not blocked, and its induction is not upregulated. This means that an adequate level of amino acids is available, and the cell is not experiencing unnecessary stress. This is detected by mTORC1 through the PI3K/Akt pathway; mTORC1 then phosphorylates and inhibits ULK1. ULK1 is then unable to phosphorylate and activate a complex of Beclin-1 and VPS34, and autophagy is not induced further than basal levels. In the basal levels of autophagy that does occur, phosphorylation of the VPS34/Beclin-1 complex by ULK1 results in the initiation of autophagy, leading to the creation of precursor vesicles which form into pre-autophagosome structures. P62 tags and delivers unwanted cellular substrates to the forming autophagosome. The pre-autophagosome then matures into an autophagosome, engulfing the p62-tagged substrates. The autophagosome fuses with a lysosome to form an autophagolysosome (also known as autolysosome). In the autolysosome, the substrates along with p62 are degraded. B) In Sandhoff mice and C2C12 cells with lysosomal enzyme knockdown, autophagy was induced greater than basal levels and was found to be blocked. A deficiency of amino acids or cellular stress affects the ATP:AMP ratio of the cell, which is detected by AMPK. Under these conditions, mTORC1 is inhibited and AMPK phosphorylates and activates ULK1, which initiates induction of autophagy. ULK1 activates the Beclin-1/VPS34 complex, which initiates the formation of pre-cursor vesicles that form into the pre-autophagosome and engulfs p62-tagged substrates. One theory for the block of autophagy and the accumulation of p62 is that the pre-autophagosomes are able to mature into autophagosomes but are unable to properly fuse with lysosomes to form autolysosomes. Another theory of for the block in autophagy is that pre-autophagosomes are unable to mature properly into autophagosomes, resulting in the accumulation of p62 and autophagic vacuoles.

Inhibition of Myogenesis in LSDs

Western blot analysis of lysates from Sandhoff mice soleus muscles showed a significant decrease in expression of myogenin and MHC compared to wild-type mice (Fig. 5). A similar observation was found in our C2C12 cells which were transfected with siRNA to knockdown specific lysosomal enzymes and differentiated for 120h (Fig. 8). Our results agree with a previous study showing undetectable myogenin staining and weak embryonic MHC expression in patients of another LSD, Pompe disease (Schaaf et al., 2015). Our observations indicate that a deficiency of Neu1, *Hexb*, or β-gal results in the reduced expression of muscle regulatory factors essential to terminal myogenic differentiation (Fig. 14). Since myogenin activates myotube formation through the fusion of myoblasts, a decrease in myogenin expression would result in reduced fusion of myoblasts and a reduction in myotube formation (Zanou and Gailly, 2013). Furthermore, a lack of myogenin has been observed to prevent formation of myofibers (Bharathy et al., 2013). A decrease in MHC expression suggests a defective terminal myogenic differentiation and muscle regeneration (Schaaf et al., 2015). This is because muscle growth, especially during the early stages after birth, and the ability of muscles to regenerate is highly dependent on myogenesis (Maltzahn et al., 2013). If the muscles are unable to regenerate, then injury and damage to muscle tissue cannot be repaired leading to progressive muscle loss.

Our cell counting and immunocytochemistry analysis on our C2C12 cells yielded similar results. The percentage of multinucleated myotubes over the total number of cells for each treatment was significantly decreased in the lysosomal knockdown cells compared to the negative control cells (Fig. 9). When myoblasts fuse into myotubes they become

multinucleated; as myogenesis progresses these myotubes further recruit new myoblasts and form large cells with many nuclei (Champigny et al., 2005). Thus, the decrease in multinucleated myotubes suggests that the knockdown of lysosomal enzymes Neu1, *Hexb* and β-gal, results in a reduction in fusion of myoblasts and further validates in impairment in myogenic differentiation. Immunocytochemistry images of differentiated C2C12 myoblasts showed that myogenin and MHC-positive myotubes in lysosomal knockdown cells were less abundant, had fewer nuclei, and were smaller than negative control cells (Fig. 10 & 11). These results indicate that lysosomal knockdown of these lysosomal enzymes results in a defect in myoblast fusion, a reduced ability of formed myotubes to recruit new myoblasts, and the favoured formation of smaller myotubes with less nuclei. A defect in myotube formation would lead to impaired synthesis of new myofibers and negatively impact muscle tissue.

In Pompe disease, the skeletal muscle pathology which included muscle fiber vacuolization, and loss of cross striation, was attributed to failed activation of pre-myoblast cells and muscle regeneration (Schaaf et al., 2015). Since myogenic differentiation plays such a vital role in muscle growth and regeneration, it can be implied that the muscle dysfunction observed in Sialidosis, Sandhoff disease, GM1-gangliosidosis, and other LSDs is caused by the impairment of myogenic differentiation that we have observed from our results (Fig. 15). It is possible that the myopathy observed in LSDs as evident through the abnormalities in the extracellular matrix, accumulation of connective tissue and vacuolization within muscle fibers, occurs because the muscles are unable to regenerate and compensate for muscle loss due to impaired myogenic differentiation.

Considering the role of autophagy during myogenic differentiation, the impairment in myogenesis could be attributed to the induction and block of autophagy we observed in our LSD models. Autophagy is required for the elimination of pre-existing organelles and myoblast remodelling during differentiation (McMillan and Quadrilatero, 2014). During myoblast fusion, it is likely that recycling of membranes, organelles and other substrates are required. This is demonstrated in studies which showed that autophagy is induced during myogenic differentiation. An increase in catabolic processes such as autophagy is required to promote cellular differentiation (McMillan and Quadrilatero, 2014). This is evident because as myogenesis progressed, p62 expression levels decreased, while the ratio of LC3-II over LC3-I significantly increased, indicating an induction of autophagy during myogenesis (McMillan and Quadrilatero, 2014). Moreover, chemical inhibition of autophagy has been observed to delay the expression of myogenin and MHC, thereby reducing myoblast fusion (McMillan and Quadrilatero, 2014). In mice with disrupted autophagy, through knockout of an autophagy gene, there was decreased levels of skeletal muscle differentiation marker, increased levels of myoD and intact levels of Myf5, suggesting a defect in differentiation and smaller myofibers (Martinez-Lopez et al., 2013). Since myoD and Myf5 expression decreases in the terminal stages of differentiation, it is possible that autophagy is required for the regulation of the expression of muscle regulatory factors (Bentzinger et al., 2012) (Fig. 14).

In muscles, impairment of autophagy has resulted in deposits and damage to the sarcolemma. Abnormal mitochondria were observed to settle between the myofibrils or beneath the sarcolemma of muscle cells when an autophagy gene was deleted (Sandri,

2010). Consequently, invaginations within the sarcolemma occurred in mice lacking the lysosomal enzyme, Neu1 (Zanoteli et al., 2010. This resulted in connective tissue infiltrates occurring in between myofiber tissues (Zanoteli et al., 2010). Since the satellite cells necessary for myogenesis to occur are located between the sarcolemma and basal lamina, it provides further evidence that a deficiency of lysosomal enzymes and the accompanying block in autophagy can potentiate the muscle dysfunction observed in LSD patients (Bharathy et al., 2013).

Hence, from our results it can be implied that the block of autophagy, observed in our models of Sialidosis, Sandhoff disease, and GM1-gangliosidosis, inhibited myoblast fusion and impaired myogenic differentiation. This impairment of myogenesis in combination with the other consequences of autophagy impairment, such as accumulation of toxic substrates, results in the muscle dysfunction observed in LSDs.

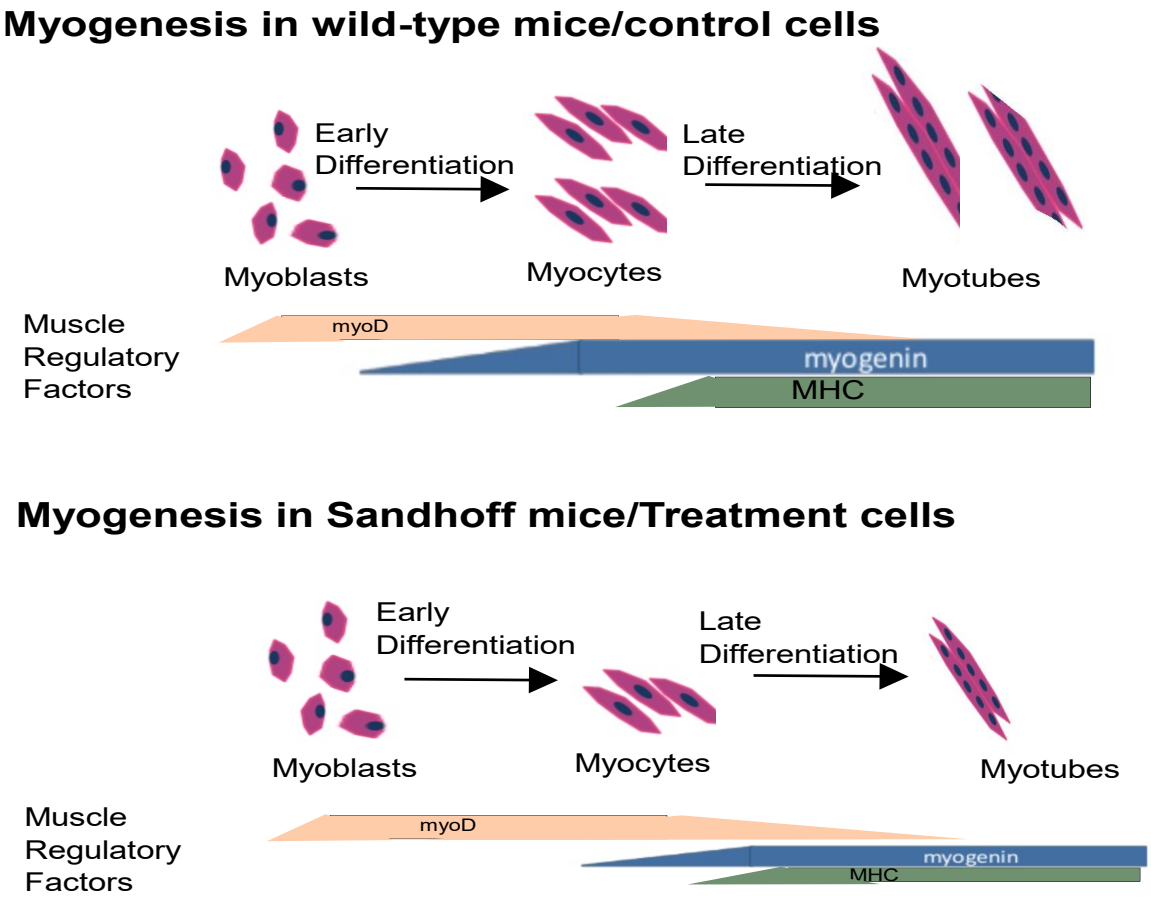

Figure 14. Expression of myogenin and MHC is reduced in Sandhoff mice and C2C12 cells with lysosomal enzyme knockdowns. This results in defective myoblast fusion and impairment in myogenic differentiation. In wild-type mice (*Hexb*$^{+/+}$) and control C2C12 cells, myoD expression is induced by the Pax3 and Pax7 transcription factors (Zanou and Gailly, 2013). myoD ceases myoblast proliferation and initiates migration and differentiation. In later stages of differentiation, myoD expression decreases. Myogenin expression is then induced in order to activate myoblast fusion. In the terminal stages of differentiation, MHC is also expressed. Long, multinucleated myotubes are then formed. However, during myogenic differentiation in Sandhoff mice and C2C12 cells with lysosomal knockdown, myogenin and MHC expression is significantly reduced. This results in reduced fusion of myoblasts, leading to reduced formation of myotubes. The myotubes that do form are much smaller and contain less nuclei.

Conclusion

In this study we have shown that autophagy is induced and blocked in Sialidosis, Sandhoff disease and GM1-gangliosidosis. We have also shown that expression of muscle regulatory factors, essential to the terminal stages of myogenesis, is significantly decreased, and myoblast fusion and myogenic differentiation is impaired. Considering the importance of autophagy during myogenesis, our results suggests that autophagy and myogenic differentiation are interrelated in LSDs. Thus, we proposed that the induction and block of autophagy in LSDs disrupts myogenic differentiation, which potentiates muscle dysfunction (Fig. 15). These findings present a new insight on how deficiencies of lysosomal enzymes impact the cell. Most of the research on this topic has been focused solely on the effect of LSDs on single pathways. The autophagic pathway is emerging as a vital regulator of muscle mass, however the mechanisms on the interrelation between autophagic and myogenic pathways is still unclear. Our study has revealed how these pathways may impact each other in LSD individuals.

Studies have observed common neurological, muscular and skeletal features between LSDs and neurodegenerative diseases such as Alzheimer's Disease and Parkinson's (Keilani et al., 2012). Therefore, studies such as this one can be extended to other diseases in which the autophagic pathway is involved. Our study highlights autophagy as a pathway of interest and as a therapeutic target for research and treatment of diseases associated with muscle dysfunction.

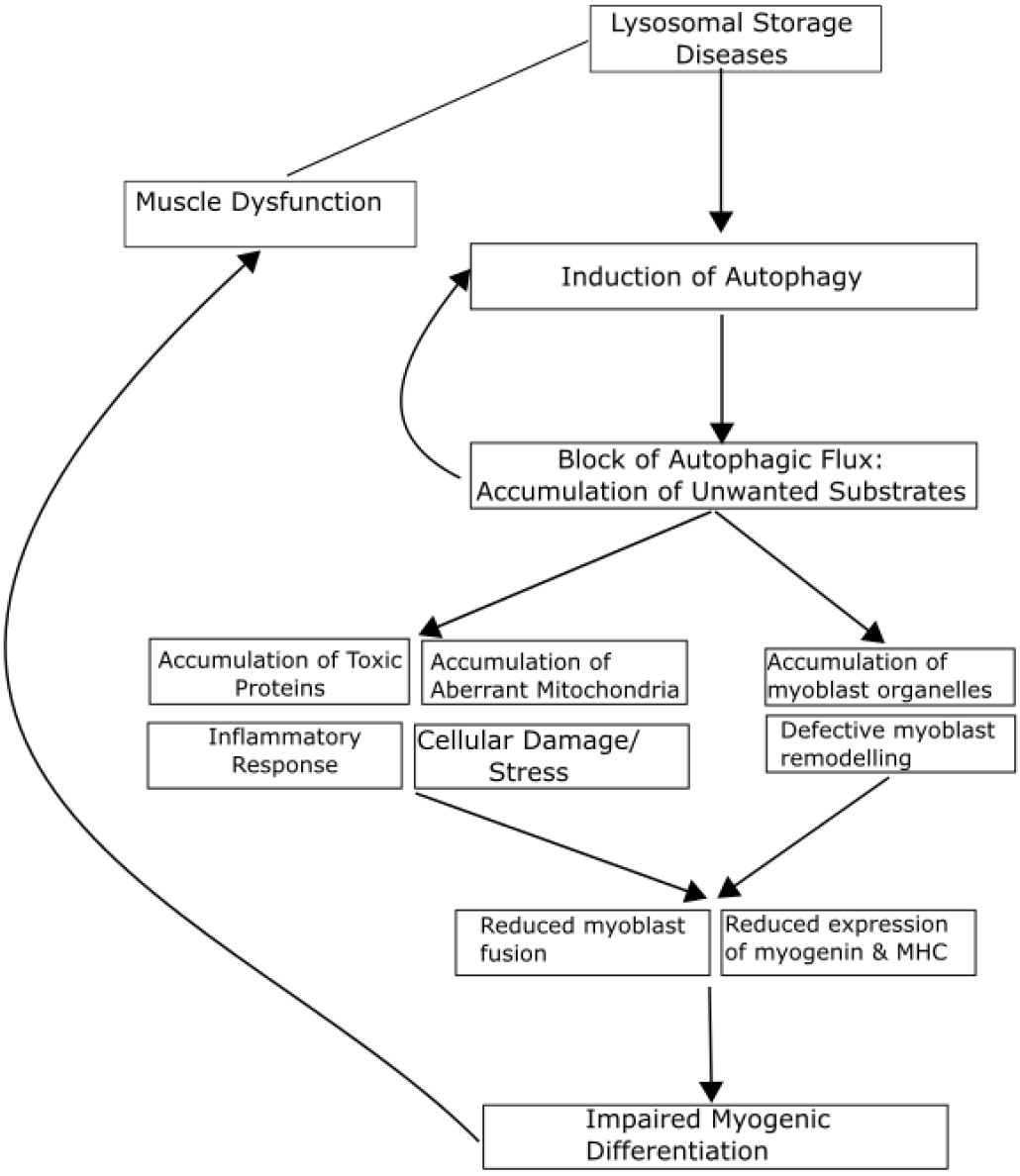

Figure 15. Proposed model of the impact of autophagy on myogenic differentiation and muscle dysfunction in LSDs. Muscle dysfunction is a common manifestation observed in a number of LSDs. It can range from muscle weakness to muscle atrophy or degeneration of muscle fibers. In LSDs, our results suggest that the induction and block of autophagy is responsible for this muscle dysfunction. We propose that this block of autophagy results in a negative feedback which causes further upregulation of autophagic induction. This block of autophagy also leads to the accumulation of toxic proteins and aberrant mitochondria, which induces an inflammatory response and further potentiates cellular damage and stress. A block of autophagy also results in the accumulation of unwanted myoblast substrates and defective myoblast remodelling during myogenic differentiation. These consequences of autophagic impairment contribute to reduced myoblast fusion and expression of myogenin and MHC, ultimately leading to impaired myogenic differentiation. This defect in myogenesis then potentiates muscle dysfunction.

References

Ballabio, A., & Gieselmann, V. (2009). Lysosomal disorders: from storage to cellular damage. Biochim Biophys Acta, 1793(4), 684-696. doi: 10.1016/j.bbamcr.2008.12.001

Bentzinger, C. F., Wang, Y. X., & Rudnicki, M. A. (2012). Building muscle: molecular regulation of myogenesis. Cold Spring Harb Perspect Biol, 4(2).

Bernard, M., Dieude, M., Yang, B., Hamelin, K., Underwood, K., & Hebert, M. J. (2014). Autophagy fosters myofibroblast differentiation through MTORC2 activation and downstream upregulation of CTGF. Autophagy, 10(12), 2193-2207.

Bharathy, N., Ling, B. M., & Taneja, R. (2013). Epigenetic regulation of skeletal muscle development and differentiation. Subcell Biochem, 61, 139-150.

Bonaldo, P., & Sandri, M. (2013). Cellular and molecular mechanisms of muscle atrophy. Dis Model Mech, 6(1), 25-39.

Bonten, E. J., Annunziata, I., & d'Azzo, A. (2014). Lysosomal multienzyme complex: pros and cons of working together. Cellular and Molecular Life Sciences, 71(11), 2017-2032.

Bostner, J., Karlsson, E., Pandiyan, M. J., Westman, H., Skoog, L., Fornander, T., . . . Stal, O. (2013). Activation of Akt, mTOR, and the estrogen receptor as a signature to predict tamoxifen treatment benefit. Breast Cancer Res Treat, 137(2), 397-406.

Brunetti-Pierri, N., & Scaglia, F. (2008). GM1 gangliosidosis: review of clinical, molecular, and therapeutic aspects. Mol Genet Metab, 94(4), 391-396.

Carpenter, S., & Karpati, G. (1986). Lysosomal storage in human skeletal muscle. Hum Pathol, 17(7), 683-703.

Carroll, B., & Dunlop, E. A. (2017). The lysosome: a crucial hub for AMPK and mTORC1 signalling. Biochem J, 474(9), 1453-1466.

Champigny, M. J., Perry, R., Rudnicki, M., & Igdoura, S. A. (2005). Overexpression of MyoD-inducible lysosomal sialidase (neu1) inhibits myogenesis in C2C12 cells. Exp Cell Res, 311(1), 157-166.

Chang, N. C., Chevalier, F. P., & Rudnicki, M. A. (2016). Satellite Cells in Muscular Dystrophy - Lost in Polarity. Trends Mol Med, 22(6), 479-496.

Chiricozzi, E., Niemir, N., Aureli, M., Magini, A., Loberto, N., Prinetti, A., . . . Sonnino, S. (2014). Chaperone therapy for GM2 gangliosidosis: effects of pyrimethamine on beta-hexosaminidase activity in Sandhoff fibroblasts. Mol Neurobiol, 50(1), 159-167.

D'Azzo, A., Machado, E., & Annunziata, I. (2015). Pathogenesis, emerging therapeutic targets and treatment in sialidosis. Expert Opinion on Orphan Drugs, 3(5), 491-504.

Dunlop, E. A., & Tee, A. R. (2013). The kinase triad, AMPK, mTORC1 and ULK1, maintains energy and nutrient homoeostasis. Biochem Soc Trans, 41(4), 939-943.

Dunlop, E. A., & Tee, A. R. (2014). mTOR and autophagy: a dynamic relationship governed by nutrients and energy. Semin Cell Dev Biol, 36, 121-129.

Fanzani, A., Zanola, A., Faggi, F., Papini, N., Venerando, B., Tettamanti, G., . . . Monti, E. (2012). Implications for the mammalian sialidases in the physiopathology of skeletal muscle. Skelet Muscle, 2(1), 23.

Fortini, P., Ferretti, C., Iorio, E., Cagnin, M., Garribba, L., Pietraforte, D., . . . Dogliotti, E. (2016). The fine tuning of metabolism, autophagy and differentiation during in vitro myogenesis. Cell Death Dis, 7, e2168.

Franceschetti, S., & Canafoglia, L. (2016). Sialidoses. Epileptic Disord, 18(S2), 89-93.

Ha, J., Guan, K. L., & Kim, J. (2015). AMPK and autophagy in glucose/glycogen metabolism. Mol Aspects Med, 46, 46-62.

Hooper, A. W. M., Alamilla, J. F., Venier, R. E., Gillespie, D. C., & Igdoura, S. A. (2017). Neuronal pentraxin 1 depletion delays neurodegeneration and extends life in Sandhoff disease mice. Hum Mol Genet, 26(4), 661-673.

Jeyakumar, M., Butters, T. D., Cortina-Borja, M., Hunnam, V., Proia, R. L., Perry, V. H., . . . Platt, F. M. (1999). Delayed symptom onset and increased life expectancy in Sandhoff disease mice treated with N-butyldeoxynojirimycin. Proceedings of the National Academy of Sciences, 96(11), 6388-6393.

Keilani, S., Lun, Y., Stevens, A. C., Williams, H. N., Sjoberg, E. R., Khanna, R., . . . Gandy, S. (2012). Lysosomal dysfunction in a mouse model of Sandhoff disease leads to accumulation of ganglioside-bound amyloid-beta peptide. J Neurosci, 32(15), 5223-5236.

Laplante, M., & Sabatini, D. M. (2012). mTOR signaling in growth control and disease. Cell, 149(2), 274-293.

Lieberman, A. P., Puertollano, R., Raben, N., Slaugenhaupt, S., Walkley, S. U., & Ballabio, A. (2012). Autophagy in lysosomal storage disorders. Autophagy, 8(5), 719-730.

Magini, A., Polchi, A., Tancini, B., Urbanelli, L., Hasilik, A., & Emiliani, C. (2012). Glycohydrolases beta-hexosaminidase and beta-galactosidase are associated with lipid microdomains of Jurkat T-lymphocytes. Biochimie, 94(3), 684-694.

Martinez-Lopez, N., Athonvarangkul, D., Sahu, S., Coletto, L., Zong, H., Bastie, C. C., . . . Singh, R. (2013). Autophagy in Myf5+ progenitors regulates energy and glucose

homeostasis through control of brown fat and skeletal muscle development. EMBO Rep, 14(9), 795-803.

Masiero, E., Agatea, L., Mammucari, C., Blaauw, B., Loro, E., Komatsu, M., . . . Sandri, M. (2009). Autophagy is required to maintain muscle mass. Cell Metab, 10(6), 507-515.

McMillan, E. M., & Quadrilatero, J. (2014). Autophagy is required and protects against apoptosis during myoblast differentiation. Biochem J, 462(2), 267-277.

Mendoza, M. C., Er, E. E., & Blenis, J. (2011). The Ras-ERK and PI3K-mTOR pathways: cross-talk and compensation. Trends Biochem Sci, 36(6), 320-328.

Menzies, F. M., Fleming, A., & Rubinsztein, D. C. (2015). Compromised autophagy and neurodegenerative diseases. Nat Rev Neurosci, 16(6), 345-357.

Mony, V. K., Benjamin, S., & O'Rourke, E. J. (2016). A lysosome-centered view of nutrient homeostasis. Autophagy, 12(4), 619-631.

Napolitano, G., & Ballabio, A. (2016). TFEB at a glance. 129(13), 2475-2481.

Neves Jde, C., Rizzato, V. R., Fappi, A., Garcia, M. M., Chadi, G., van de Vlekkert, D., . . . Zanoteli, E. (2015). Neuraminidase-1 mediates skeletal muscle regeneration. Biochim Biophys Acta, 1852(9), 1755-1764.

Newton, P. T., Vuppalapati, K. K., Bouderlique, T., & Chagin, A. S. (2015). Pharmacological inhibition of lysosomes activates the MTORC1 signaling pathway in chondrocytes in an autophagy-independent manner. Autophagy, 11(9), 1594-1607.

Otomo, T., Higaki, K., Nanba, E., Ozono, K., & Sakai, N. (2009). Inhibition of autophagosome formation restores mitochondrial function in mucolipidosis II and III skin fibroblasts. Mol Genet Metab, 98(4), 393-399.

Parenti, G., Andria, G., & Ballabio, A. (2015). Lysosomal storage diseases: from pathophysiology to therapy. Annu Rev Med, 66, 471-486.

Parkinson-Lawrence, E. J., Shandala, T., Prodoehl, M., Plew, R., Borlace, G. N., & Brooks, D. A. (2010). Lysosomal storage disease: revealing lysosomal function and physiology. Physiology (Bethesda), 25(2), 102-115.

Peker, N., Donipadi, V., Sharma, M., McFarlane, C., & Kambadur, R. (2018). Loss of Parkin impairs mitochondrial function and leads to muscle atrophy. Am J Physiol Cell Physiol, 315(2), C164-c185.

Phaneuf, D., Wakamatsu, N., Huang, J. Q., Borowski, A., Peterson, A. C., Fortunato, S. R., . . . Gravel, R. A. (1996). Dramatically different phenotypes in mouse models of human Tay-Sachs and Sandhoff diseases. Hum Mol Genet, 5(1), 1-14.

Pierson, T. M., Torres, P. A., Zeng, B. J., Glanzman, A. M., Adams, D., Finkel, R. S., . . . Kolodny, E. H. (2013). Juvenile-onset motor neuron disease caused by novel mutations in beta-hexosaminidase. Mol Genet Metab, 108(1), 65-69.

Poewe, W., Seppi, K., Tanner, C. M., Halliday, G. M., Brundin, P., Volkmann, J., . . . Lang, A. E. (2017). Parkinson disease. Nat Rev Dis Primers, 3, 17013.

Prada, C. E., & Grabowski, G. A. (2013). Neuronopathic lysosomal storage diseases: Clinical and pathologic findings. Developmental Disabilities Research Reviews, 17(3), 226-246.

Prater, S. N., Patel, T. T., Buckley, A. F., Mandel, H., Vlodavski, E., Banugaria, S. G., . . . Kishnani, P. S. (2013). Skeletal muscle pathology of infantile Pompe disease during long-term enzyme replacement therapy. Orphanet J Rare Dis, 8, 90. 10.1186/1750-1172-8-90

Sandri, M. (2010). Autophagy in skeletal muscle. FEBS letters,584(7), 1411-1416.

Sandri, M. (2011). New findings of lysosomal proteolysis in skeletal muscle. Curr Opin Clin Nutr Metab Care, 14(3), 223-229.

Sandri, M. (2013). Protein breakdown in muscle wasting: role of autophagy-lysosome and ubiquitin-proteasome. Int J Biochem Cell Biol, 45(10), 2121-2129.

Sango, K., McDonald, M. P., Crawley, J. N., Mack, M. L., Tifft, C. J., Skop, E., . . . Proia, R. L. (1996). Mice lacking both subunits of lysosomal beta-hexosaminidase display gangliosidosis and mucopolysaccharidosis. Nat Genet, 14(3), 348-352.

Saxton, R. A., & Sabatini, D. M. (2017). mTOR Signaling in Growth, Metabolism, and Disease. Cell, 168(6), 960-976.

Schaaf, G. J., van Gestel, T. J., Brusse, E., Verdijk, R. M., de Coo, I. F., van Doorn, P. A., . . . Pijnappel, W. W. (2015). Lack of robust satellite cell activation and muscle regeneration during the progression of Pompe disease. Acta Neuropathol Commun, 3, 65.

Schiaffino, S., Dyar, K. A., Ciciliot, S., Blaauw, B., & Sandri, M. (2013). Mechanisms regulating skeletal muscle growth and atrophy. Febs j, 280(17), 4294-4314.

Schnaar, R. L., Suzuki, A., & Stanley, P. (2009). Glycosphingolipids. In nd, A. Varki, R. D. Cummings, J. D. Esko, H. H. Freeze, P. Stanley, C. R. Bertozzi, G. W. Hart & M. E. Etzler (Eds.), Essentials of Glycobiology. Cold Spring Harbor (NY): Cold Spring Harbor Laboratory Press.The Consortium of Glycobiology Editors, La Jolla, California.

Settembre, C., Zoncu, R., Medina, D. L., Vetrini, F., Erdin, S., Erdin, S., . . . Ballabio, A. (2012). A lysosome-to-nucleus signalling mechanism senses and regulates the lysosome via mTOR and TFEB. Embo j, 31(5), 1095-1108. doi: 10.1038/emboj.2012.32

Sincennes, M. C., Brun, C. E., & Rudnicki, M. A. (2016). Concise Review: Epigenetic Regulation of Myogenesis in Health and Disease. Stem Cells Transl Med, 5(3), 282-290.

Skop, V., Cahova, M., Dankova, H., Papackova, Z., Palenickova, E., Svoboda, P., . . . Kazdova, L. (2014). Autophagy inhibition in early but not in later stages prevents 3T3-L1 differentiation: Effect on mitochondrial remodeling. Differentiation, 87(5), 220-229.

Takamura, A., Higaki, K., Kajimaki, K., Otsuka, S., Ninomiya, H., Matsuda, J., . . . Nanba, E. (2008). Enhanced autophagy and mitochondrial aberrations in murine G(M1)-gangliosidosis. Biochem Biophys Res Commun, 367(3), 616-622.

Tanaka, Y., Guhde, G., Suter, A., Eskelinen, E. L., Hartmann, D., Lullmann-Rauch, R., . . . Saftig, P. (2000). Accumulation of autophagic vacuoles and cardiomyopathy in LAMP-2-deficient mice. Nature, 406(6798), 902-906.

Vergarajauregui, S., & Puertollano, R. (2008). Mucolipidosis type IV: the importance of functional lysosomes for efficient autophagy. Autophagy, 4(6), 832-834.

Ward, C., Martinez-Lopez, N., Otten, E. G., Carroll, B., Maetzel, D., Singh, R., . . . Korolchuk, V. I. (2016). Autophagy, lipophagy and lysosomal lipid storage disorders. Biochim Biophys Acta, 1861(4), 269-284.

Yoon, M. S., & Chen, J. (2013). Distinct amino acid-sensing mTOR pathways regulate skeletal myogenesis. Mol Biol Cell, 24(23), 3754-3763.

Yoshida, K., Oshima, A., Sakuraba, H., Nakano, T., Yanagisawa, N., Inui, K., . . . et al. (1992). GM1 gangliosidosis in adults: clinical and molecular analysis of 16 Japanese patients. Ann Neurol, 31(3), 328-332.

Yu, X., & Long, Y. C. (2015). Autophagy modulates amino acid signaling network in myotubes: differential effects on mTORC1 pathway and the integrated stress response. Faseb j, 29(2), 394-407.

Yusuf, F., & Brand-Saberi, B. (2012). Myogenesis and muscle regeneration. Histochem Cell Biol, 138(2), 187-199.

Zanoteli, E., van de Vlekkert, D., Bonten, E. J., Hu, H., Mann, L., Gomero, E. M., . . . d'Azzo, A. (2010). Muscle degeneration in neuraminidase 1-deficient mice results from infiltration of the muscle fibers by expanded connective tissue. Biochim Biophys Acta, 1802(7-8), 659-672.

Zanou, N., & Gailly, P. (2013). Skeletal muscle hypertrophy and regeneration: interplay between the myogenic regulatory factors (MRFs) and insulin-like growth factors (IGFs) pathways. Cell Mol Life Sci, 70(21), 4117-4130.